

Superlight pairs in face-centred-cubic extended Hubbard models with strong Coulomb repulsion

G D Adebajo^{1,*} , P E Kornilovitch²  and J P Hague^{1,*} 

¹ School of Physical Sciences, The Open University, Walton Hall, Milton Keynes, MK7 6AA, United Kingdom

² Department of Physics, Oregon State University, Corvallis, OR, 97331, United States of America

E-mail: ganiyu.adebanjo@gmail.com and jim.hague@open.ac.uk

Received 1 October 2021, revised 14 December 2021

Accepted for publication 5 January 2022

Published 19 January 2022



Abstract

The majority of fulleride superconductors with unusually high transition-temperature to kinetic-energy ratios have a face-centred-cubic (FCC) structure. We demonstrate that, within extended Hubbard models with strong Coulomb repulsion, paired fermions in FCC lattices have qualitatively different properties than pairs in other three-dimensional cubic lattices. Our results show that strongly bound, light, and small pairs can be generated in FCC lattices across a wide range of the parameter space. We estimate that such pairs can Bose condense at high temperatures even if the lattice constant is large (as in the fullerenes).

Keywords: extended Hubbard models, superlight fermion pairs, superconductivity, Bose–Einstein condensation, face-centred cubic lattice, unconventional superconductivity, UV model

(Some figures may appear in colour only in the online journal)

1. Introduction

Superlight small pairs are of interest in the context of superconductivity due to their potential to form Bose–Einstein condensates (BEC) at high temperatures [1, 2]. There are a number of low-dimensional systems within which superlight pair states can be realised, for example the staggered ladder [2], triangular lattice [1, 3] and quasi-two-dimensional hexagonal lattice [4]. Pairs consisting of two fermions can be bound onto neighbouring sites by a combination of strong intersite attraction and strong onsite repulsion. Such pairs can be light and small (superlight) if it is possible to move to neighbouring lattice sites via a single hop without breaking the pairing [2], so


that the pair motion is a first order effect. In many materials there is a strong onsite Coulomb repulsion, so intersite pairs are formed via any intersite or long-range attraction, which could originate either from phonons or other more exotic mechanisms. The aim of this article is to explore the possibility of superlight small pairs in face-centred cubic (FCC) lattices.

Extended Hubbard models [5, 6] contain the essential interactions to realise superlight states. The Hamiltonian of an extended Hubbard model is defined as:

$$H = \sum_{\langle \mathbf{n}, \mathbf{a} \rangle \sigma} t_{\mathbf{a}} c_{\mathbf{n}+\mathbf{a}, \sigma}^{\dagger} c_{\mathbf{n} \sigma} + U \sum_{\mathbf{n}} \hat{\rho}_{\mathbf{n} \uparrow} \hat{\rho}_{\mathbf{n} \downarrow} + \sum_{\langle \mathbf{n}, \mathbf{a} \rangle} V \hat{\rho}_{\mathbf{n}+\mathbf{a}} \hat{\rho}_{\mathbf{n}}, \quad (1)$$

where $c_{\mathbf{n} \sigma}^{\dagger}$ ($c_{\mathbf{n} \sigma}$) creates (annihilates) an electron of spin σ at site \mathbf{n} , $\hat{\rho}_{\mathbf{n}} = \hat{\rho}_{\mathbf{n} \uparrow} + \hat{\rho}_{\mathbf{n} \downarrow}$, where $\hat{\rho}_{\mathbf{n} \sigma}$ is the number operator for electrons on site \mathbf{n} with spin σ , \mathbf{a} is the intersite lattice vector, $t_{\mathbf{a}}$ is the intersite hopping, U is the onsite interaction and V is the intersite interaction. Both U and V may be attractive or repulsive, although in most materials repulsive U is more likely due to the difficulties of overcoming the Hubbard U with

* Authors to whom any correspondence should be addressed.

 Original content from this work may be used under the terms of the [Creative Commons Attribution 4.0 licence](https://creativecommons.org/licenses/by/4.0/). Any further distribution of this work must maintain attribution to the author(s) and the title of the work, journal citation and DOI.

attractive interactions, such as those due to electron–phonon interactions. In the low-density limit the model is also known as the UV model. Properties of local pairs, which can be used to estimate the Bose–Einstein condensation temperature, have been studied in simple systems using the UV model [4, 7–10]. If U is highly repulsive and V is attractive, then superlight pairs can be found on suitable lattices.

Extended Hubbard models have been extensively applied to the quasi-2D cuprate superconductors [11, 12]. The origin of an intersite V can be from Coulomb repulsion, long range electron–phonon interactions [13], and an intersite J can originate from anti-ferromagnetic interactions induced by the Hubbard U [14]. Various phases are predicted in extended Hubbard models, such as spin triplet pairing [15], d -wave superconductivity [12], Mott insulators [16], XY antiferromagnetism [17] and stripe order [18]. We note that experimental evidence for strong intersite attractions mediated by phonons has been reported recently in one-dimensional cuprates [19, 20].

In FCC lattices, electrons paired between near-neighbour sites can move with a single hop. An illustration of such pair movement in an FCC lattice is shown in figure 1. If sufficient intersite attraction is present, and there is repulsive Hubbard U to suppress on-site pairing, the pair can move easily through the lattice. This should result in a low effective pair mass for small pairs, which could in turn yield a high transition temperature. To our knowledge, superlight pairs have not yet been examined in FCC systems. The complexity of the FCC lattice structure and increased number of nearest-neighbour sites complicate the calculation and we aim to fill this gap. The detailed calculations presented in this paper explore how pair properties evolve with Hubbard U and V in FCC lattices, and identify regions of the parameter space where pairs are small and light.

The microscopic understanding of complex phases in strongly correlated systems remains a challenge. There are many numerical techniques that are suitable for treating strongly correlated systems, including extended Hubbard models. These include exact diagonalisation (ED) [21], density matrix renormalisation group (DMRG) and matrix product state calculations [22, 23], dynamical mean-field theory (DMFT), its extensions dynamical cluster approximation, cellular DMFT, and extended DMFT to treat extended Hubbard models [12, 24–27], quantum Monte Carlo (QMC) techniques [1], and recently quantum embedding [28–30] and machine learning algorithms [31]. Many of these techniques are limited to 1D and 2D systems, either inherently, or because particle numbers are limited. The exponentially growing Hilbert space limits ED to small numbers of sites and particles, effectively limiting application to 1D and small 2D systems. DMRG and MPS work best in 1D. QMC techniques can suffer from sign problems when the number of particles becomes large, although the number of sites may not be limited. On the other hand, DMFT is most accurate for large spatial dimensions, although the coarse graining of the self-energy removes some details of the lattice [24]. The integration of DMFT and density functional theory calculations has led to powerful techniques for the simulation of materials [32].

In spite of their ubiquity in condensed matter systems, FCC lattices are often overlooked within the correlated electrons community owing to their relative complexity compared to other lattices. Materials of interest with FCC lattices include the A_3C_{60} compounds: a family of molecular compounds with high transition temperature [33] (where A is an alkali metal e.g. K, Rb, Cs) which are predominantly FCC structured [34]. In addition to electron–phonon interactions [33] found in these alkali-doped compounds, strong correlation [35] is also prevalent. The presence of long-range phonon mediated interactions (e.g. the intermolecular modes [34, 36]) may lead to suitable conditions for extended Hubbard physics and superlight pairs could also be relevant to other FCC materials.

This work aims to provide an exact solution of the two-electron problem in an FCC lattice. We calculate the critical potentials U_c (V_c) to bind particles into pairs, the system’s total energy, the pair’s size and mass, and BEC transition temperatures of pairs in the low-density (dilute) limit. The paper is organised as follows: we describe the model Hamiltonian and methodology used to solve the UV model in the dilute limit (section 2). In section 3, the properties of the formed pairs are reported. We conclude this work with a discussion in section 4.

2. Methodology

We find the exact solution to a single-orbital system of two spin 1/2 fermions where the orbital energy is taken to be zero. The two-body problem relevant to the Hamiltonian in equation (1) must satisfy the equation below:

$$\sum_{\mathbf{a}} t_{\mathbf{a}} [\Psi(\mathbf{n}_1 + \mathbf{a}, \mathbf{n}_2) + \Psi(\mathbf{n}_1, \mathbf{n}_2 + \mathbf{a})] + \sum_{\mathbf{a}} \hat{V}_{\mathbf{a}} \delta_{\mathbf{n}_1 - \mathbf{n}_2, \mathbf{a}} \Psi(\mathbf{n}_1, \mathbf{n}_2) = E \Psi(\mathbf{n}_1, \mathbf{n}_2). \quad (2)$$

Here E is the total energy of the system, $\Psi(\mathbf{n}_1, \mathbf{n}_2)$ is the real-space wave function of the fermions, and \mathbf{n}_1 and \mathbf{n}_2 are the spatial coordinates. $\hat{V}_{\mathbf{a}}$ combines the interaction terms into a single function with $\hat{V}_{r=0} = U$ and $\hat{V}_{r=\mathbf{a}} = V$. The wave function in Fourier space is

$$\psi_{\mathbf{k}_1 \mathbf{k}_2} = \frac{1}{N} \sum_{\mathbf{n}_1 \mathbf{n}_2} \Psi(\mathbf{n}_1, \mathbf{n}_2) e^{-i\mathbf{k}_1 \mathbf{n}_1 - i\mathbf{k}_2 \mathbf{n}_2}, \quad (3)$$

where N is the total number of lattice points. Substituting the inverse of equation (3) into equation (2) gives:

$$(E - \varepsilon_{\mathbf{k}_1} - \varepsilon_{\mathbf{k}_2}) \psi_{\mathbf{k}_1 \mathbf{k}_2} = \frac{1}{N} \sum_{\mathbf{a}\mathbf{q}} \hat{V}_{\mathbf{a}} e^{i(\mathbf{q}-\mathbf{k}_1)\mathbf{a}} \psi_{\mathbf{q}, \mathbf{k}_1 + \mathbf{k}_2 - \mathbf{q}}, \quad (4)$$

where \mathbf{k} is the particle’s momentum vector.

The dispersion relation in the FCC lattice is given as

$$\varepsilon_{\mathbf{k}} = -4t \left[\cos \frac{k_x b}{2} \cdot \cos \frac{k_y b}{2} + \cos \frac{k_y b}{2} \cdot \cos \frac{k_z b}{2} + \cos \frac{k_x b}{2} \cdot \cos \frac{k_z b}{2} \right], \quad (5)$$

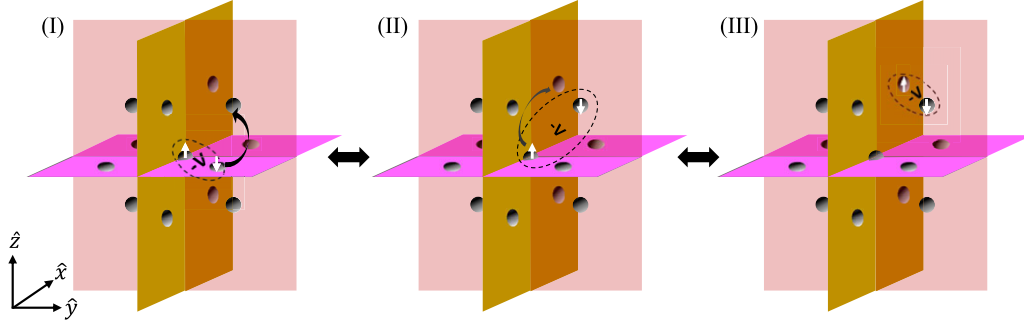


Figure 1. Schematic demonstrating the first-order hopping of superlight small pairs on the FCC lattice. The white vertical arrow represents an electron with its spin, each small gray circle is a lattice site (only the 13 sites of interest are shown), the dashed oval represents a bound state through an attractive V , the curved arrow represents electron hopping, and the two-way arrow implies that the configurations are degenerate. The key feature here is that the pair is itinerant as long as the intersite interaction is sufficiently attractive, and there is sufficient Hubbard U to stop on-site pairs from forming. Unlike in other cubic lattices where first-order superlight states are only attainable via an attractive U , the superlight state in the FCC lattice corresponds to a more physical case where the local Coulomb repulsion is large.

where b is the lattice constant.

The solution to the problem involves 13 self-consistent algebraic equations. We apply (anti-)symmetrisation to separate the symmetric (singlet) states from the anti-symmetric (triplet) states. Following reference [10], the (anti-)symmetrised wave function is expressed as

$$\begin{aligned} (E - \varepsilon_{\mathbf{k}_1} - \varepsilon_{\mathbf{k}_2})\phi_{\mathbf{k}_1\mathbf{k}_2}^\pm &= \frac{1}{N} \sum'_{\mathbf{q}\mathbf{a}} \hat{V}_{\mathbf{a}} \{e^{i(\mathbf{q}-\mathbf{k}_1)\mathbf{a}} \pm e^{i(\mathbf{q}-\mathbf{k}_2)\mathbf{a}}\} \phi_{\mathbf{q},\mathbf{k}_1+\mathbf{k}_2-\mathbf{q}}^\pm, \end{aligned} \quad (6)$$

where

$$\phi_{\mathbf{k}_1\mathbf{k}_2}^\pm = \psi_{\mathbf{k}_1\mathbf{k}_2} \pm \psi_{\mathbf{k}_2\mathbf{k}_1}, \quad (7)$$

and $+$ and $-$ refer to the singlet and the triplet wave functions, respectively. The summation over the lattice vector, \mathbf{a} , in equation (6) is split into two sets: $\{\mathbf{a}_+\}$ for singlets, and $\{\mathbf{a}_-\}$ for triplets. We define them as

$$\begin{aligned} \{\mathbf{a}_+\} = & \left\{ (0, 0, 0), \left(\frac{b}{2}, \frac{b}{2}, 0\right), \left(0, \frac{b}{2}, \frac{b}{2}\right), \left(\frac{b}{2}, 0, \frac{b}{2}\right), \right. \\ & \left. \left(\frac{b}{2}, -\frac{b}{2}, 0\right), \left(0, \frac{b}{2}, -\frac{b}{2}\right), \left(-\frac{b}{2}, 0, \frac{b}{2}\right) \right\}, \end{aligned} \quad (8)$$

$$\begin{aligned} \{\mathbf{a}_-\} = & \left\{ \left(\frac{b}{2}, \frac{b}{2}, 0\right), \left(0, \frac{b}{2}, \frac{b}{2}\right), \left(\frac{b}{2}, 0, \frac{b}{2}\right), \left(\frac{b}{2}, -\frac{b}{2}, 0\right), \right. \\ & \left. \left(0, \frac{b}{2}, -\frac{b}{2}\right), \left(-\frac{b}{2}, 0, \frac{b}{2}\right) \right\}, \end{aligned} \quad (9)$$

where, again, b is the lattice constant. The primed summation in equation (6) means that a factor of $1/2$ should be included for the case $\mathbf{a}_+ = 0$. If we define a function

$$\Phi_{\mathbf{a}_\pm}^\pm(\mathbf{k}_1 + \mathbf{k}_2) = \Phi_{\mathbf{a}_\pm}^\pm(\mathbf{P}) \equiv \frac{1}{N} \sum_{\mathbf{q}} e^{i\mathbf{q}\mathbf{a}_\pm} \phi_{\mathbf{q},\mathbf{P}-\mathbf{q}}^\pm, \quad (10)$$

where $\mathbf{P} = \mathbf{k}_1 + \mathbf{k}_2$ is the total momentum of the particle pair, then, $\phi_{\mathbf{k}_1\mathbf{k}_2}^\pm$ in equation (6) can be expressed in terms of $\Phi_{\mathbf{a}_\pm}^\pm$.

Replacing $\phi_{\mathbf{q},\mathbf{P}-\mathbf{q}}^\pm$ in equation (10) leads to the self-consistent equations

$$\Phi_{\mathbf{a}_\pm}^\pm(\mathbf{P}) = - \sum_{\mathbf{a}'_\pm} \hat{V}_{\mathbf{a}'_\pm} L_{\mathbf{a}_\pm\mathbf{a}'_\pm}^\pm(E, \mathbf{P}) \Phi_{\mathbf{a}'_\pm}^\pm(\mathbf{P}), \quad (11)$$

where

$$L_{\mathbf{a}_\pm\mathbf{a}'_\pm}^\pm(E, \mathbf{P}) = \frac{1}{N} \sum_{\mathbf{q}} \frac{e^{i\mathbf{q}(\mathbf{a}_\pm - \mathbf{a}'_\pm)} \pm e^{i[\mathbf{q}\mathbf{a}_\pm - (\mathbf{P}-\mathbf{q})\mathbf{a}'_\pm]}}{-E + \varepsilon_{\mathbf{q}} + \varepsilon_{\mathbf{P}-\mathbf{q}}}, \quad (12)$$

is the Green's function of the lattice. The full dispersion matrices for the singlets and triplets can be found in appendix A and all calculations are at zero temperature. In the thermodynamic limit (infinite lattice size), equation (12) is a generalised Watson integral that in 3D converges for any energy that's below the threshold energy of $-2W$.

3. Results

3.1. Total energy

The ground state energy can be used to identify whether two particles are bound or not. At zero momentum and zero temperature, the threshold energy of two unbound particles is $E^{\text{Th}} = -2W$, where $W = 12t$ is the half-bandwidth. The total energy in figure 2 shows all the different pair symmetries found in the FCC lattice. The particles are unbound when there is a plateau at $-2W$ and the energy drops below this threshold value when the particles bind.

A critical attraction must be reached before the formation of any bound state. At very large attractions U and V , the s -states have very similar values (insets of figures 2(a) and (b)). In figure 2(b), the s -states are formed at relatively weak intersite attractions V compared to other states. Additionally, for very strong attractive V , the energies of all the pair symmetries are separated by an energy of order t : except for the d_{E_g} - and f -states that have approximately the same energies and are therefore indiscernible when plotted (inset of figure 2(b)). Note that the labels $d_{T_{2g}}$ and d_{E_g} are d -states with T_{2g} and E_g symmetries respectively. The separation of states at large attractive

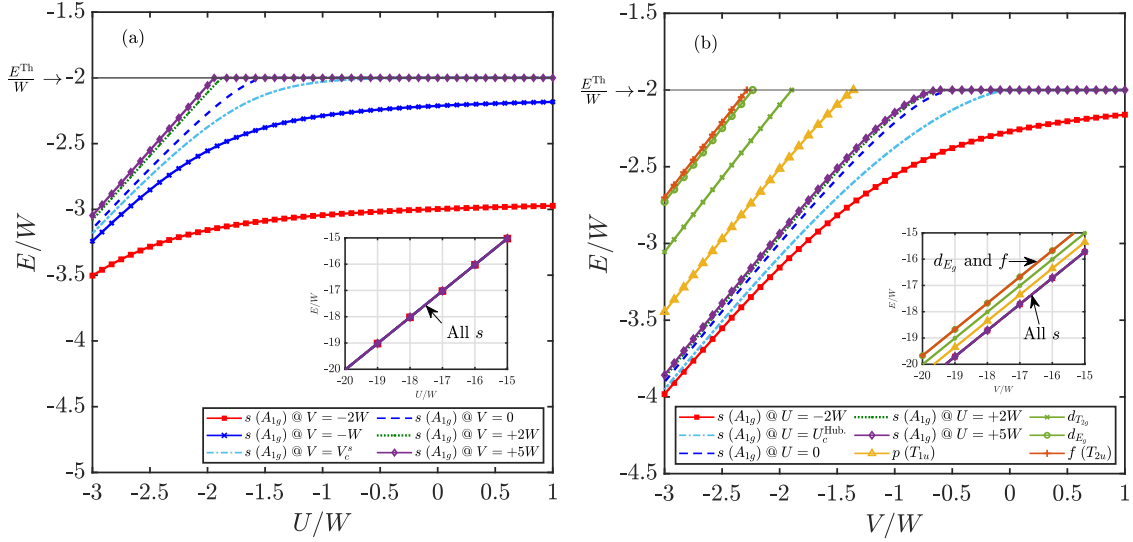


Figure 2. The total energy of pairs for (a) the s -states only, and (b) all states of various symmetries. The critical attractions for the s -state are $U_c^{\text{Hub.}}(V=0) = -1.4874W$ and $V_c^s(U=0) = -0.4836W$. All states except the s -state are unaffected by U . The excited states (p , $d_{T_{2g}}$, d_{E_g} and f) only appear at strongly attractive V . At very large attractions U and V , all s -states have similar values (insets of panels (a) and (b)). For large intersite attraction, $V \rightarrow -\infty$, the d_{E_g} and f states have approximately the same energies and are indiscernible: inset of panel (b).

V occurs because the matrix elements only depend on the hopping parameter t as $V \rightarrow -\infty$, as can be seen in equation (B9). Put another way, at deep V the particles are confined to a fixed size shell, and therefore the region of confinement, and thus the energies, become V independent. At $\mathbf{P} = 0$, the degeneracy of the p -, $d_{T_{2g}}$ -, d_{E_g} -, and f - states is three-fold, three-fold, two-fold and three-fold, respectively. Spin singlet ground states of pairs are common in Hubbard models [37].

3.2. Binding diagram

At zero pair momentum, we construct a phase diagram (figure 3) which shows where bound pairs form. States with nonzero angular momentum (i.e. p -, $d_{T_{2g}}$ -, d_{E_g} - and f - states) are insensitive to U , as evident in figure 3.

In comparison to other lattices with lower coordination numbers, pairs require stronger attractions for their formation in the FCC lattice. This is due to the increase in kinetic energy with coordination number. The critical U or V required for binding can be found analytically (refer to appendix A for more details) via

$$V_c^s(U) \leq \frac{UL_0 - 1}{UL_0C - C - 12UL_1^2}, \quad (13)$$

where $L_0 = -\sqrt{3}K_0^2/(8\pi^2t)$, $L_1 = 1/(24t) + L_0$, $C = 12L_0 + 1/(2t)$ and $K_0 = K\left(\frac{\sqrt{3}-1}{2\sqrt{2}}\right) = 1.598142\dots$ is the complete elliptic integral of the first kind. Note that equation (13) only holds when $\mathbf{P} = 0$.

The required potential to create bound onsite pairs with no intersite interaction is $U_c^{\text{Hub.}}(V=0) \approx -1.4874W$ (the negative Hubbard model, $V=0$). This is a slightly greater attraction relative to the simple cubic [9] and body-centred cubic [10] lattices. Equation (13) also yields the critical attraction $V_c^s(U=0) \approx -0.4836W$. At infinite intersite repulsion, the onsite s -state is guaranteed to form if

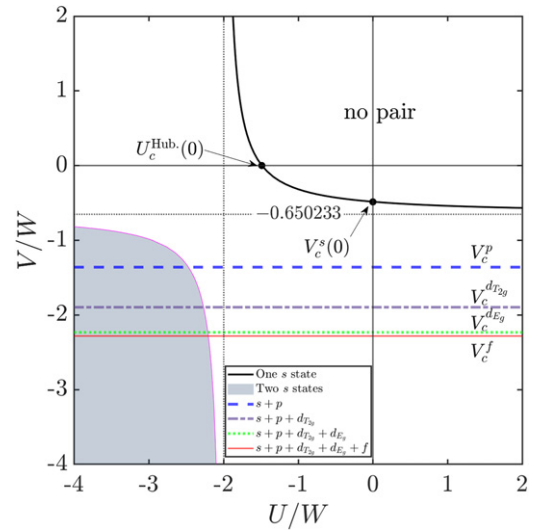


Figure 3. Binding diagram showing pair formation at $\mathbf{P} = 0$ in an FCC lattice. The top (black) curved line is the boundary that separates bound from unbound s -symmetry pairs, the (grey) shaded region enclosed by the (magenta) solid line indicates a region with two s -states, the (blue) thick dashed line represents the onset of triply degenerate p -states, the (purple) dash-dotted line shows the binding of a triple degenerate d -symmetry pair of T_{2g} symmetry (labelled $d_{T_{2g}}$), the (green) dotted line is the line below which two d -wave pairs with E_g symmetry start to form (labelled d_{E_g}) and the (red) solid line indicates the formation of a triply-degenerate f pairs. An s -state is guaranteed to form for attractions equal to or stronger than $U = -2W$, $V = -0.65023W$. The boundaries are exact to at least eight significant figures.

$U_c^{\text{Hub.}}(V \rightarrow +\infty) \leq -2W$. Also, $V_c^s(+\infty) = -0.6502W$. The non- s pairs have critical intersite binding strength $V_c^p \approx -1.3586W$, $V_c^{dT_{2g}} \approx -1.8945W$, $V_c^{dE_g} \approx -2.2342W$, $V_c^f \approx -2.2847W$.

Table 1. Comparing critical binding strengths at $\mathbf{P} = 0$ in 3D cubic lattices (simple cubic, body-centered cubic, FCC). $W_S = 6t$, $W_B = 8t$, and $W_F = 12t$ are the respective half-bandwidths. We note that there are more pairing states in the FCC lattice than the other lattices.

Pairing symmetry	Binding parameter	Minimum attraction required		
		SC	BCC	FCC
<i>s</i> -wave	$U(V = 0)$	$-1.3189W_S$	$-1.4355W_B$	$-1.4874W_F$
	$U(V = +\infty)$	$-2W_S$	$-2W_B$	$-2W_F$
	$V(U = 0)$	$-0.6455W_S$	$-0.6358W_B$	$-0.4836W_F$
	$V(U = +\infty)$	$-0.9789W_S$	$-0.8858W_B$	$-0.6502W_F$
<i>p</i> -wave (A_{2u})	V	$-1.5885W_S$	$-1.5828W_B$	$-1.3586W_F$
<i>d</i> -wave (T_{2g})	V		$-1.8804W_B$	$-1.8945W_F$
<i>d</i> -wave (E_g)	V	$-1.8034W_S$		$-2.2342W_F$
<i>f</i> -wave (T_{2u})	V		$-1.9639W_B$	$-2.2847W_F$

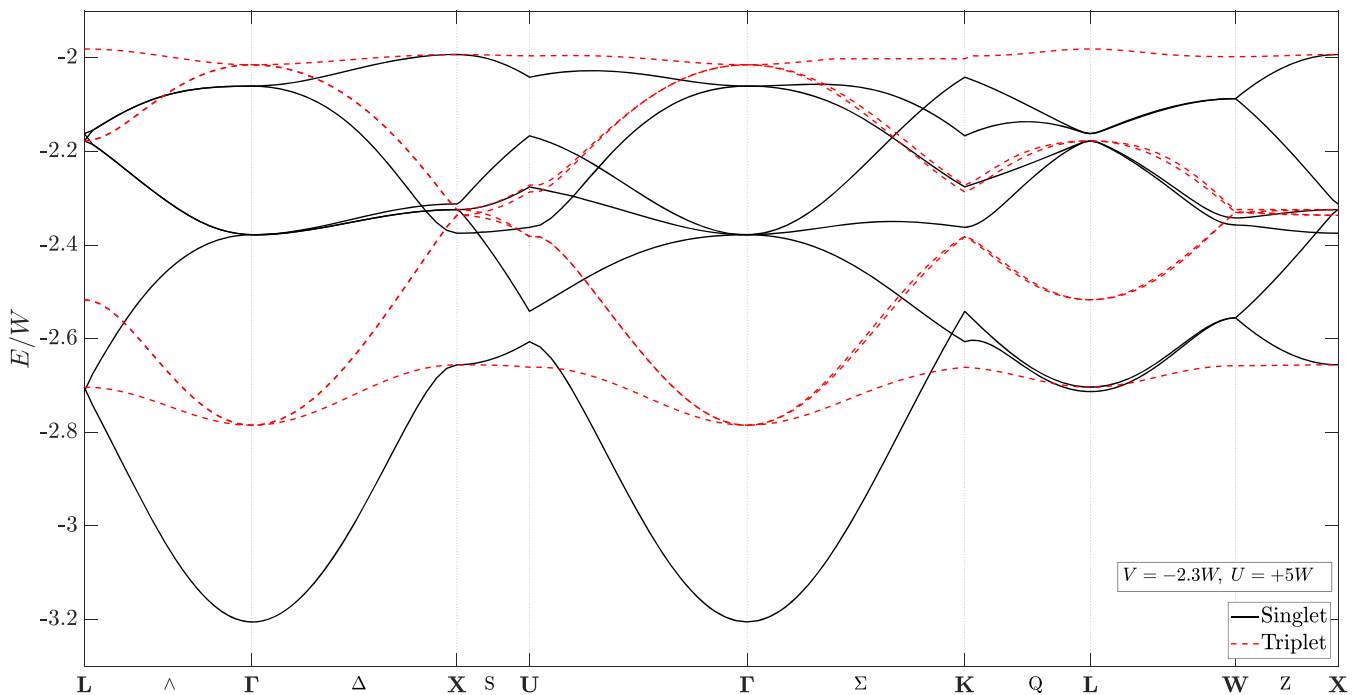


Figure 4. Dispersion curve of bound pairs at $U = +5W$ and $V = -2.3W$. Moving away from the Γ point, degeneracies are lifted. Spin triplets are identified with a dashed (red) curve and spin singlets with solid (black) curve.

If measured in terms of their respective bandwidths, there are similarities in the critical attractions needed to bind two fermions in the simple cubic, BCC and FCC lattices. The summary of this comparison is given in table 1.

3.3. Dispersion

The pair energy at non-zero momentum is needed to estimate the pair mass. The dispersion of singlet and triplet states across the FCC Brillouin zone (BZ) for $U = +5W$ (repulsive) and $V = -2.3W$ (attractive) is shown in figure 4. To observe the dispersion of the excited states (d_{E_g} and f), an intersite interaction stronger than the bandwidth ($-2W$) is required (evident from table 1). Away from the Γ point, degeneracies are lifted and there are mixing and crossing of states, making it difficult to specify pair symmetries. However, our method guarantees unambiguous classification of singlets and triplets. The overall

form of the dispersions has been confirmed at strong coupling with perturbation theory calculations (see appendix B).

3.4. Pair mass

The effective mass is calculated from the second derivative of the pair energy dispersion as

$$[m_i^*]^{-1} = \frac{1}{\hbar^2} \frac{\partial^2 E}{\partial P_i^2}, \quad (14)$$

and masses can be seen in figure 5.

In some lattices (e.g. rectangular ladder [1], simple cubic [9], and BCC [10]), a superlight itinerant state is formed only when U and V are nearly equal and are both attractive, which enhances the mobility of the pair via a single hop. However,

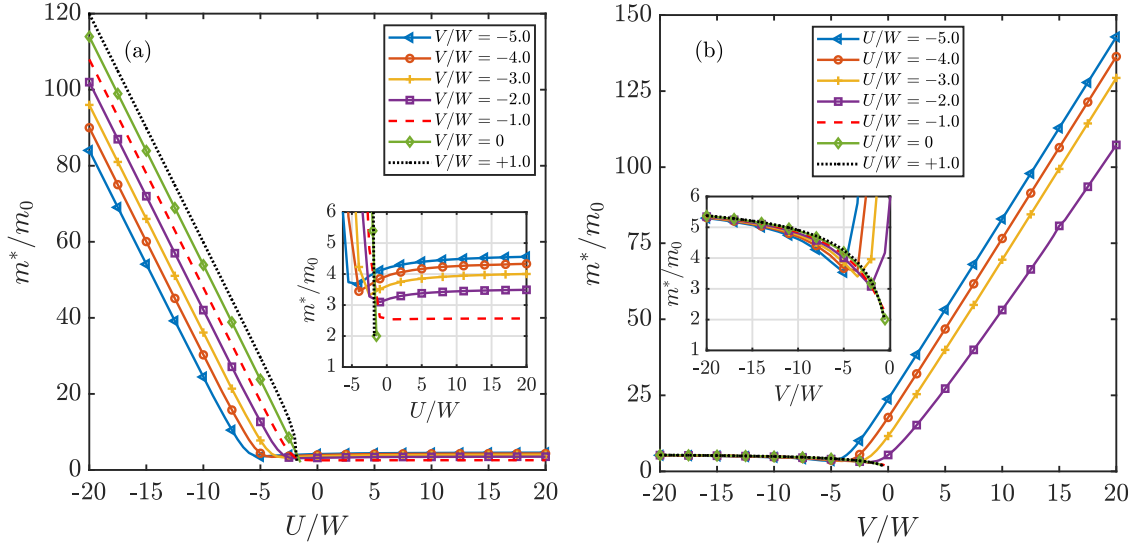


Figure 5. Dependence of the pair mass on (a) U , (b) V . Pair mass increases with large and attractive U . In the limit $V \rightarrow -\infty$, the geometry of the FCC lattice means the pair mass tends to a value six times heavier than a single particle (inset of panel (b)).

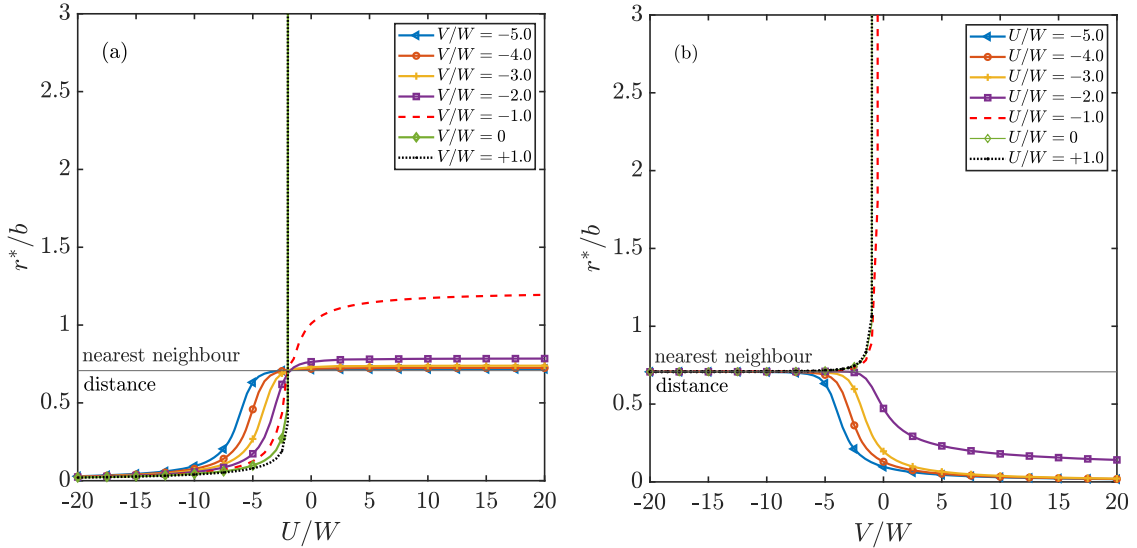


Figure 6. Radius in units of the lattice constant for (a) onsite interaction at different V , (b) intersite interaction for various U . The radius diverges at the binding threshold. Intersite pairs form when V is attractive and dominates, but when attractive Hubbard U dominates, the formation of an onsite pair is favoured.

for superlight pairs in staggered ladder [2] and triangular lattices [3], attractive onsite attraction is not required: a condition which is closer to physical systems which typically have onsite repulsion. The FCC lattice, due to its structure, belongs to the latter group.

In the limit where the intersite interaction is attractive and dominant $V \rightarrow -\infty$, the pair mass (figure 5(b)) tends to $m^* = 6m_0$ (see appendix B for perturbation theory calculations in the large attractive V limit) since the movement of the pair only depends linearly on t . On the other hand, in the limit where the onsite attraction is largely dominant $U \rightarrow -\infty$ and V is small or repulsive, the mass of the bound pair increases with $|U|$. In this case, the pair movement is second-order in the hopping parameter t , with pair mass increasing with $|U|$, because

it is necessary to hop through a higher energy intersite state for motion to occur.

3.5. Pair radius

The effective radius is obtained from the expression

$$\langle r^* \rangle = \sqrt{\frac{\sum_{\mathbf{n}} \mathbf{n}^2 \Psi^*(\mathbf{n}_1, \mathbf{n}_2) \Psi(\mathbf{n}_1, \mathbf{n}_2)}{\sum_{\mathbf{n}} \Psi^*(\mathbf{n}_1, \mathbf{n}_2) \Psi(\mathbf{n}_1, \mathbf{n}_2)}}, \quad (15)$$

where $\mathbf{n} = |\mathbf{n}_1 - \mathbf{n}_2|$. The radius is plotted in figure 6.

The size of the pair diverges near the threshold energy ($E \rightarrow E^{\text{Th}}$). This is because the pair is weakly bound and the pair wave function spreads over distant lattice sites. If the

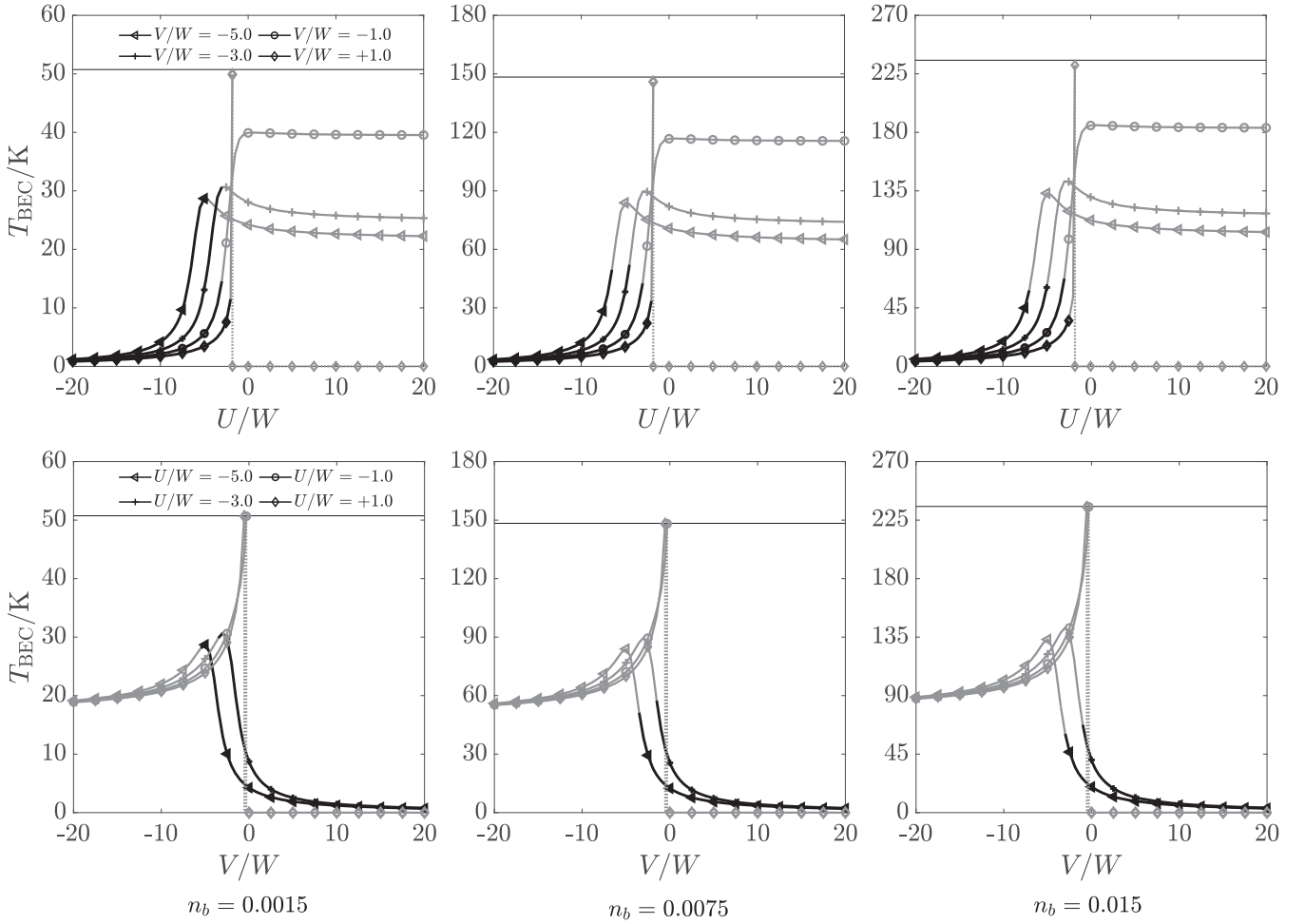


Figure 7. Plots of BEC transition temperature for bound pairs in the dilute limit. The number of pairs per site n_b increases from left to right. Dark lines are used if n_b satisfies the pair overlap condition. We observe a region of constant T_{BEC} in the superlight regimes. The horizontal lines show T_{BEC} for pairs of mass $m^* = 2m_0$. The dotted regions (abrupt decrease to zero transition temperature) indicate $T_{\Delta} < T_{\text{BEC}}$ (so there are no preformed pairs).

particles unbind, the size becomes infinite. When V is strongly attractive and dominates over U , we see the formation of a local intersite pair, with size on the order of the lattice parameter. In contrast, if the Hubbard attraction is very strong and dominant, an onsite pair is formed.

3.6. Bose–Einstein condensation

We estimate BEC transition temperatures for pairs in an FCC lattice, obtained from the Bose integral as,

$$T_{\text{BEC}} = \frac{3.31\hbar^2}{m_b^*k_{\text{B}}} \left(\frac{n_b}{\Omega_{\text{site}}} \right)^{2/3}, \quad (16)$$

where $\Omega_{\text{site}} = b^3/4$ is the volume of the Wigner–Seitz cell for the FCC lattice and n_b is the number of pairs per lattice site. We use lattice constant $b = 14.24 \text{ \AA}$ as an example (consistent with the FCC fullerenes, although we note that electrons are not dilute in fullerenes and further manipulations would be required to derive a UV model for such materials). Transition temperatures for fixed n_b are plotted in figure 7. For BEC to take place at T_{BEC} , pairs must exist above T_{BEC} , such that $T_{\text{BEC}} < T_{\Delta}$, where $T_{\Delta} = \Delta/k_{\text{B}}$ is the

pairing temperature and binding energy $\Delta = 2\varepsilon_0 - E_0$. The value $t = 0.04 \text{ eV}$ (consistent with fulleride superconductors [34]) is used to set the energy scale. The maximum n_b for which T_{BEC} is consistent with the effective mass approximation is estimated to be approximately 0.015. We require that pairs of radius $R' = \alpha r^*$ can fit into space without overlapping, so $n_b 16R'^3/3 < 1$. Selecting $\alpha = 5$ is suggested to minimise the overlap of wave functions of different pairs to $\sim 1\%$. For $n_b = 0.0015$, $T_{\text{BEC}} \lesssim 30 \text{ K}$ and for $n_b = 0.015$ $T_{\text{BEC}} \lesssim 70 \text{ K}$.

4. Discussion and conclusions

This paper explored the formation and properties of fermion pairs in an FCC lattice. The binding diagram, pair energy, effective mass and radius were calculated, and BEC transition temperatures were estimated. When the intersite attraction is large and U is repulsive, leading to strongly bound intersite pairs, the bound pair was found to be six times heavier than a single particle mass, since geometric properties of FCC lattices allow motion of strongly bound intersite pairs as a first order effect. Infinitely heavy pairs are found on the FCC lattice for $U \rightarrow -\infty$.

Intersite pair motion on FCC lattices differs qualitatively from other 3D cubic lattices, where either next-nearest neighbour hopping or attractive Hubbard $U \sim V$ would be required to form light states when V is strong and attractive. While effective attractive U could be created if a very strong electron–phonon interaction overcome the Hubbard U , this would lead to very heavy pairs due to polaron effects. The geometric properties of FCC lattices which do not require the electron–phonon interaction to overcome the Hubbard U , could lead to pairs, created by intersite electron–phonon interactions (and other mechanisms) that are light, mobile and undergo a superconducting transition at high temperatures.

It is possible to measure the mass of carriers in cuprate superconductors using optical and Hall measurements. This shows that in the quasi-2D high temperature superconductors, typical carrier masses are three electron masses, so light carriers are not necessarily unique to FCC lattices, and can be found if the intersite attraction is weak [14, 38]. We note that superlight states may not correspond to the highest transition temperatures for FCC lattices, and we estimate slightly higher T_{BEC} for weakly bound pairs. What is unusual here is that the pair masses are small, *both* when the intersite attraction is weak *and* when it is strong, which might allow superconductivity to be found at higher temperatures in a wider range of the parameter space of the extended Hubbard model on FCC lattices (perhaps making it easier to find materials with the right properties for superconductivity). We also note that it might be possible to probe the carrier mass in FCC fullerenes using similar optical and Hall measurements.

Optical lattices may offer an alternative way to measure the properties of superlight pairs, since the mass enhancement of six in the strong attraction limit is a feature of the lattice geometry. FCC optical lattices can be formed using arrangements of four laser beams [39, 40]. The Hubbard U in such systems can be controlled via the Feshbach resonance. Intersite V is formed using dressed Rydberg states, and can be controlled using the principal quantum number for the Rydberg states and the detuning from the Rydberg state. In practice, FCC optical lattices have large lattice constants so we expect the BEC temperature will be low. However it may be possible to observe superlight pairs in optical lattice experiments in the normal state.

Further investigations using other theoretical techniques would be of interest. The challenge is to find techniques that can deal with the FCC structures without losing the detail of the lattice. For small numbers of particles, path integral QMC could be used [1], but ED would not be appropriate in 3D as lattice sizes would be limited to less than four sites across due to the 4^N growth in Hilbert space. Approaching the thermodynamic limit is a challenge. DMFT is most suitable for 3D systems, but the coarse graining of the BZ washes out details of the lattice, such that results for all 3D lattices would be qualitatively identical. We note that transition temperatures predicted here are similar to those in FCC fullerene materials. While the fullerenes are not dilute, we suggest that future work could also include a determination of an effective UV Hamiltonian for light doping away from half filling in such systems.

Data availability statement

All data that support the findings of this study are included within the article (and any supplementary files).

Appendix A. UV model on FCC lattice

A.1. Schrödinger equation

The (anti-)symmetrised Schrödinger equation can be written as,

$$(E - \varepsilon_{\mathbf{k}_1} - \varepsilon_{\mathbf{k}_2})\phi_{\mathbf{k}_1\mathbf{k}_2}^{\pm} = \frac{1}{N} \sum'_{\mathbf{q}\mathbf{a}_{\pm}} \hat{V}_{\mathbf{a}_{\pm}} \{e^{i(\mathbf{q}-\mathbf{k}_1)\mathbf{a}_{\pm}} \pm e^{i(\mathbf{q}-\mathbf{k}_2)\mathbf{a}_{\pm}}\} \phi_{\mathbf{q},\mathbf{k}_1+\mathbf{k}_2-\mathbf{q}}^{\pm}. \quad (\text{A1})$$

The prime in the summation means that a factor of $\frac{1}{2}$ must be included for the case $\mathbf{a}_+ = 0$. Spin singlets have solutions belonging to the symmetrised Schrödinger equation while spin triplets can be found from the anti-symmetrised version of equation (A1).

We define the vectors for the singlets and triplets respectively as

$$\begin{aligned} \{\mathbf{a}_+\} &= \{\mathbf{a}_0^+, \mathbf{a}_1^+, \mathbf{a}_2^+, \mathbf{a}_3^+, \mathbf{a}_4^+, \mathbf{a}_5^+, \mathbf{a}_6^+\} = \{(0, 0, 0), \\ &(\frac{1}{2}, \frac{1}{2}, 0), (0, \frac{1}{2}, \frac{1}{2}), (\frac{1}{2}, 0, \frac{1}{2}), (\frac{1}{2}, -\frac{1}{2}, 0), (0, \frac{1}{2}, -\frac{1}{2}), (-\frac{1}{2}, 0, \frac{1}{2})\} \\ \{\mathbf{a}_-\} &= \{\mathbf{a}_1^-, \mathbf{a}_2^-, \mathbf{a}_3^-, \mathbf{a}_4^-, \mathbf{a}_5^-, \mathbf{a}_6^-\} = \{(\frac{1}{2}, \frac{1}{2}, 0), (0, \frac{1}{2}, \frac{1}{2}), \\ &(\frac{1}{2}, 0, \frac{1}{2}), (\frac{1}{2}, -\frac{1}{2}, 0), (0, \frac{1}{2}, -\frac{1}{2}), (-\frac{1}{2}, 0, \frac{1}{2})\}. \end{aligned}$$

In this section, we set $b = 1$.

A.1.1. Symmetrised Schrödinger equation. Using the vectors $\{\mathbf{a}_+\}$ in equation (A1), we obtain

$$\begin{aligned} (E - \varepsilon_{\mathbf{k}_1} - \varepsilon_{\mathbf{k}_2})\phi_{\mathbf{k}_1\mathbf{k}_2}^+ &= \frac{1}{N} \sum_{\mathbf{q}} \left[\frac{1}{2} U \left(e^{i(\mathbf{q}-\mathbf{k}_1)\mathbf{a}_0^+} \right. \right. \\ &+ e^{i(\mathbf{q}-\mathbf{k}_2)\mathbf{a}_0^+} \left. \right) + V(e^{i(\mathbf{q}-\mathbf{k}_1)\mathbf{a}_1^+} + e^{i(\mathbf{q}-\mathbf{k}_2)\mathbf{a}_1^+}) \\ &+ V(e^{i(\mathbf{q}-\mathbf{k}_1)\mathbf{a}_2^+} + e^{i(\mathbf{q}-\mathbf{k}_2)\mathbf{a}_2^+}) + V(e^{i(\mathbf{q}-\mathbf{k}_1)\mathbf{a}_3^+} + e^{i(\mathbf{q}-\mathbf{k}_2)\mathbf{a}_3^+}) \\ &+ V(e^{i(\mathbf{q}-\mathbf{k}_1)\mathbf{a}_4^+} + e^{i(\mathbf{q}-\mathbf{k}_2)\mathbf{a}_4^+}) + V(e^{i(\mathbf{q}-\mathbf{k}_1)\mathbf{a}_5^+} + e^{i(\mathbf{q}-\mathbf{k}_2)\mathbf{a}_5^+}) \\ &+ V(e^{i(\mathbf{q}-\mathbf{k}_1)\mathbf{a}_6^+} + e^{i(\mathbf{q}-\mathbf{k}_2)\mathbf{a}_6^+}) \left. \right] \phi_{\mathbf{q},\mathbf{k}_1+\mathbf{k}_2-\mathbf{q}}^+ \\ &= \frac{1}{N} \sum_{\mathbf{q}} \left[U + V e^{i(\frac{q_x}{2} + \frac{q_y}{2})} (e^{-i\mathbf{k}_1\mathbf{a}_1^+} + e^{-i\mathbf{k}_2\mathbf{a}_1^+}) \right. \\ &+ V e^{i(\frac{q_y}{2} + \frac{q_z}{2})} (e^{-i\mathbf{k}_1\mathbf{a}_2^+} + e^{-i\mathbf{k}_2\mathbf{a}_2^+}) \\ &+ V e^{i(\frac{q_x}{2} + \frac{q_z}{2})} (e^{-i\mathbf{k}_1\mathbf{a}_3^+} + e^{-i\mathbf{k}_2\mathbf{a}_3^+}) \\ &+ V e^{i(\frac{q_x}{2} - \frac{q_y}{2})} (e^{-i\mathbf{k}_1\mathbf{a}_4^+} + e^{-i\mathbf{k}_2\mathbf{a}_4^+}) \\ &+ V e^{i(\frac{q_y}{2} - \frac{q_z}{2})} (e^{-i\mathbf{k}_1\mathbf{a}_5^+} + e^{-i\mathbf{k}_2\mathbf{a}_5^+}) \\ &+ V e^{i(-\frac{q_x}{2} + \frac{q_z}{2})} (e^{-i\mathbf{k}_1\mathbf{a}_6^+} + e^{-i\mathbf{k}_2\mathbf{a}_6^+}) \left. \right] \phi_{\mathbf{q},\mathbf{k}_1+\mathbf{k}_2-\mathbf{q}}^+. \quad (\text{A2}) \end{aligned}$$

The following basis functions can be used:

$$\begin{aligned}
\Phi_0^+(\mathbf{P}) &= \frac{1}{N} \sum_{\mathbf{q}} \phi_{\mathbf{q}, \mathbf{P}-\mathbf{q}}^+, \\
\Phi_1^+(\mathbf{P}) &= \frac{1}{N} \sum_{\mathbf{q}} e^{i\left(\frac{q_x}{2} + \frac{q_y}{2}\right)} \phi_{\mathbf{q}, \mathbf{P}-\mathbf{q}}^+, \\
\Phi_2^+(\mathbf{P}) &= \frac{1}{N} \sum_{\mathbf{q}} e^{i\left(\frac{q_y}{2} + \frac{q_z}{2}\right)} \phi_{\mathbf{q}, \mathbf{P}-\mathbf{q}}^+, \\
\Phi_3^+(\mathbf{P}) &= \frac{1}{N} \sum_{\mathbf{q}} e^{i\left(\frac{q_x}{2} + \frac{q_z}{2}\right)} \phi_{\mathbf{q}, \mathbf{P}-\mathbf{q}}^+, \\
\Phi_4^+(\mathbf{P}) &= \frac{1}{N} \sum_{\mathbf{q}} e^{i\left(\frac{q_x}{2} - \frac{q_y}{2}\right)} \phi_{\mathbf{q}, \mathbf{P}-\mathbf{q}}^+, \\
\Phi_5^+(\mathbf{P}) &= \frac{1}{N} \sum_{\mathbf{q}} e^{i\left(\frac{q_y}{2} - \frac{q_z}{2}\right)} \phi_{\mathbf{q}, \mathbf{P}-\mathbf{q}}^+, \\
\Phi_6^+(\mathbf{P}) &= \frac{1}{N} \sum_{\mathbf{q}} e^{i\left(-\frac{q_x}{2} + \frac{q_z}{2}\right)} \phi_{\mathbf{q}, \mathbf{P}-\mathbf{q}}^+,
\end{aligned} \tag{A3}$$

where $\mathbf{P} = \mathbf{k}_1 + \mathbf{k}_2$. The wave function in equation (A2) expressed in terms of the basis functions equation (A3) is

$$\begin{aligned}
\phi_{\mathbf{k}_1 \mathbf{k}_2}^+ &= \frac{1}{(E - \varepsilon_{\mathbf{k}_1} - \varepsilon_{\mathbf{k}_2})} \left\{ U \Phi_0^+(\mathbf{P}) + V \Phi_1^+(\mathbf{P}) \right. \\
&\times (e^{-i\mathbf{k}_1 \mathbf{a}_1^+} + e^{-i\mathbf{k}_2 \mathbf{a}_1^+}) + V \Phi_2^+(\mathbf{P}) (e^{-i\mathbf{k}_1 \mathbf{a}_2^+} + e^{-i\mathbf{k}_2 \mathbf{a}_2^+}) \\
&+ V \Phi_3^+(\mathbf{P}) (e^{-i\mathbf{k}_1 \mathbf{a}_3^+} + e^{-i\mathbf{k}_2 \mathbf{a}_3^+}) \\
&+ V \Phi_4^+(\mathbf{P}) (e^{-i\mathbf{k}_1 \mathbf{a}_4^+} + e^{-i\mathbf{k}_2 \mathbf{a}_4^+}) \\
&+ V \Phi_5^+(\mathbf{P}) (e^{-i\mathbf{k}_1 \mathbf{a}_5^+} + e^{-i\mathbf{k}_2 \mathbf{a}_5^+}) \\
&\left. + V \Phi_6^+(\mathbf{P}) (e^{-i\mathbf{k}_1 \mathbf{a}_6^+} + e^{-i\mathbf{k}_2 \mathbf{a}_6^+}) \right\}. \tag{A4}
\end{aligned}$$

Substituting equation (A4) into each entry of equation (A3) and redefining $q_j = q'_j + \frac{P_j}{2}$ leads to seven self-consistent equations. The first is

$$\begin{aligned}
\tilde{\Phi}_0^+(\mathbf{P}) &= UL_{000}(\mathbf{P})\tilde{\Phi}_0^+(\mathbf{P}) + V[L_{110}(\mathbf{P}) \\
&+ L_{\bar{1}\bar{1}0}(\mathbf{P})]\tilde{\Phi}_1^+(\mathbf{P}) \\
&+ V[L_{011}(\mathbf{P}) + L_{0\bar{1}\bar{1}}(\mathbf{P})]\tilde{\Phi}_2^+(\mathbf{P}) \\
&+ V[L_{101}(\mathbf{P}) + L_{\bar{1}0\bar{1}}(\mathbf{P})]\tilde{\Phi}_3^+(\mathbf{P}) \\
&+ V[L_{1\bar{1}0}(\mathbf{P}) + L_{\bar{1}\bar{1}0}(\mathbf{P})]\tilde{\Phi}_4^+(\mathbf{P}) \\
&+ V[L_{01\bar{1}}(\mathbf{P}) + L_{0\bar{1}\bar{1}}(\mathbf{P})]\tilde{\Phi}_5^+(\mathbf{P}) \\
&+ V[L_{\bar{1}01}(\mathbf{P}) + L_{\bar{1}0\bar{1}}(\mathbf{P})]\tilde{\Phi}_6^+(\mathbf{P}), \tag{A5}
\end{aligned}$$

where $\tilde{\Phi}_i^+(\mathbf{P}) = e^{\frac{i}{2}(\mathbf{P} \cdot \mathbf{a}_i^+)} \Phi_i^+$ (where $i = 0, 1, \dots, 6$), have phase factors which provides information about the centre-of-mass motion of the bound state. Furthermore, the L 's represent the Green's functions of the FCC lattice which are defined as

$$\begin{aligned}
L_{lmn}(\mathbf{P}) &= \frac{1}{N} \sum_{\mathbf{q}'} \frac{e^{i\left(l\frac{q'_x}{2} + m\frac{q'_y}{2} + n\frac{q'_z}{2}\right)}}{E - \varepsilon_{\frac{\mathbf{P}}{2} + \mathbf{q}'} - \varepsilon_{\frac{\mathbf{P}}{2} - \mathbf{q}'}} \\
&= - \int_{-2\pi}^{2\pi} \int_{-2\pi}^{2\pi} \int_{-2\pi}^{2\pi} \frac{dq'_x dq'_y dq'_z}{(4\pi)^3} \frac{\cos\left(l\frac{q'_x}{2} + m\frac{q'_y}{2} + n\frac{q'_z}{2}\right)}{|E| + \varepsilon_{\frac{\mathbf{P}}{2} + \mathbf{q}'} + \varepsilon_{\frac{\mathbf{P}}{2} - \mathbf{q}'}}. \tag{A6}
\end{aligned}$$

Instead of writing a negative subscript along a coordinate, we place a bar above it to keep notation compact. For the present problem where interactions are only limited to nearest-neighbour distances, l, m and n take the values 0, ± 1 , and ± 2 .

Combining all seven independent self-consistent equations for all spin-singlets at arbitrary momentum gives

$$\begin{pmatrix} UL_{000} & V[L_{110} + L_{\bar{1}\bar{1}0}] & V[L_{011} + L_{0\bar{1}\bar{1}}] & V[L_{101} + L_{\bar{1}0\bar{1}}] & V[L_{1\bar{1}0} + L_{\bar{1}\bar{1}0}] & V[L_{01\bar{1}} + L_{0\bar{1}\bar{1}}] & V[L_{\bar{1}01} + L_{\bar{1}0\bar{1}}] \\ UL_{110} & V[L_{000} + L_{220}] & V[L_{10\bar{1}} + L_{121}] & V[L_{01\bar{1}} + L_{211}] & V[L_{020} + L_{200}] & V[L_{101} + L_{12\bar{1}}] & V[L_{21\bar{1}} + L_{011}] \\ UL_{011} & V[L_{\bar{1}01} + L_{121}] & V[L_{000} + L_{022}] & V[L_{\bar{1}\bar{1}0} + L_{112}] & V[L_{\bar{1}21} + L_{101}] & V[L_{002} + L_{020}] & V[L_{110} + L_{112}] \\ UL_{101} & V[L_{0\bar{1}\bar{1}} + L_{211}] & V[L_{\bar{1}\bar{1}0} + L_{112}] & V[L_{000} + L_{202}] & V[L_{011} + L_{21\bar{1}}] & V[L_{\bar{1}\bar{1}2} + L_{110}] & V[L_{200} + L_{002}] \\ UL_{1\bar{1}0} & V[L_{0\bar{2}0} + L_{200}] & V[L_{1\bar{2}\bar{1}} + L_{101}] & V[L_{0\bar{1}\bar{1}} + L_{21\bar{1}}] & V[L_{000} + L_{220}] & V[L_{1\bar{2}1} + L_{10\bar{1}}] & V[L_{2\bar{1}\bar{1}} + L_{0\bar{1}\bar{1}}] \\ UL_{01\bar{1}} & V[L_{\bar{1}0\bar{1}} + L_{12\bar{1}}] & V[L_{002} + L_{020}] & V[L_{\bar{1}\bar{1}2} + L_{110}] & V[L_{\bar{1}2\bar{1}} + L_{10\bar{1}}] & V[L_{000} + L_{022}] & V[L_{112} + L_{110}] \\ UL_{\bar{1}01} & V[L_{2\bar{1}\bar{1}} + L_{011}] & V[L_{\bar{1}\bar{1}0} + L_{112}] & V[L_{200} + L_{002}] & V[L_{211} + L_{0\bar{1}\bar{1}}] & V[L_{\bar{1}\bar{1}2} + L_{110}] & V[L_{000} + L_{202}] \end{pmatrix} \begin{pmatrix} \tilde{\Phi}_0^+ \\ \tilde{\Phi}_1^+ \\ \tilde{\Phi}_2^+ \\ \tilde{\Phi}_3^+ \\ \tilde{\Phi}_4^+ \\ \tilde{\Phi}_5^+ \\ \tilde{\Phi}_6^+ \end{pmatrix} = \begin{pmatrix} \tilde{\Phi}_0^+ \\ \tilde{\Phi}_1^+ \\ \tilde{\Phi}_2^+ \\ \tilde{\Phi}_3^+ \\ \tilde{\Phi}_4^+ \\ \tilde{\Phi}_5^+ \\ \tilde{\Phi}_6^+ \end{pmatrix}. \tag{A7}$$

A.1.2. Anti-symmetrised Schrödinger equation. The anti-symmetrised equation is found by substituting $\{\mathbf{a}_-\}$ in equation (A1),

$$\begin{aligned}
(E - \varepsilon_{\mathbf{k}_1} - \varepsilon_{\mathbf{k}_2})\phi_{\mathbf{k}_1 \mathbf{k}_2}^- &= \frac{1}{N} \sum_{\mathbf{q}} \left[V e^{i\left(\frac{q_x}{2} + \frac{q_y}{2}\right)} (e^{-i\mathbf{k}_1 \mathbf{a}_1^-} - e^{-i\mathbf{k}_2 \mathbf{a}_1^-}) \right. \\
&+ V e^{i\left(\frac{q_y}{2} + \frac{q_z}{2}\right)} (e^{-i\mathbf{k}_1 \mathbf{a}_2^-} - e^{-i\mathbf{k}_2 \mathbf{a}_2^-}) \\
&\left. + V e^{i\left(\frac{q_x}{2} + \frac{q_z}{2}\right)} (e^{-i\mathbf{k}_1 \mathbf{a}_3^-} - e^{-i\mathbf{k}_2 \mathbf{a}_3^-}) \right.
\end{aligned}$$

$$\begin{aligned}
&+ V e^{i\left(\frac{q_x}{2} - \frac{q_y}{2}\right)} (e^{-i\mathbf{k}_1 \mathbf{a}_4^-} - e^{-i\mathbf{k}_2 \mathbf{a}_4^-}) \\
&+ V e^{i\left(\frac{q_y}{2} - \frac{q_z}{2}\right)} (e^{-i\mathbf{k}_1 \mathbf{a}_5^-} - e^{-i\mathbf{k}_2 \mathbf{a}_5^-}) \\
&\left. + V e^{i\left(-\frac{q_x}{2} + \frac{q_z}{2}\right)} (e^{-i\mathbf{k}_1 \mathbf{a}_6^-} - e^{-i\mathbf{k}_2 \mathbf{a}_6^-}) \right] \phi_{\mathbf{q}, \mathbf{k}_1 + \mathbf{k}_2 - \mathbf{q}}^-. \tag{A8}
\end{aligned}$$

Similar basis functions can be used to the singlet case:

$$\begin{aligned}\Phi_1^-(\mathbf{P}) &= \frac{1}{N} \sum_{\mathbf{q}} e^{i\left(\frac{q_x}{2} + \frac{q_y}{2}\right)} \phi_{\mathbf{q}, \mathbf{P}-\mathbf{q}}^-, \quad \Phi_2^-(\mathbf{P}) = \frac{1}{N} \sum_{\mathbf{q}} e^{i\left(\frac{q_y}{2} + \frac{q_z}{2}\right)} \phi_{\mathbf{q}, \mathbf{P}-\mathbf{q}}^- \\ \Phi_3^-(\mathbf{P}) &= \frac{1}{N} \sum_{\mathbf{q}} e^{i\left(\frac{q_x}{2} + \frac{q_z}{2}\right)} \phi_{\mathbf{q}, \mathbf{P}-\mathbf{q}}^-, \quad \Phi_4^-(\mathbf{P}) = \frac{1}{N} \sum_{\mathbf{q}} e^{i\left(\frac{q_x}{2} - \frac{q_y}{2}\right)} \phi_{\mathbf{q}, \mathbf{P}-\mathbf{q}}^- \\ \Phi_5^-(\mathbf{P}) &= \frac{1}{N} \sum_{\mathbf{q}} e^{i\left(\frac{q_y}{2} - \frac{q_z}{2}\right)} \phi_{\mathbf{q}, \mathbf{P}-\mathbf{q}}^-, \\ \Phi_6^-(\mathbf{P}) &= \frac{1}{N} \sum_{\mathbf{q}} e^{i\left(-\frac{q_x}{2} + \frac{q_z}{2}\right)} \phi_{\mathbf{q}, \mathbf{P}-\mathbf{q}}^-\end{aligned}$$

(A9) The combined self-consistent equations for all triplets are

leading to

$$\begin{aligned}\tilde{\Phi}_1^-(\mathbf{P}) &= V[L_{000} - L_{220}] \tilde{\Phi}_1^-(\mathbf{P}) \\ &+ V[L_{10\bar{1}} - L_{121}] \tilde{\Phi}_2^-(\mathbf{P}) \\ &+ V[L_{01\bar{1}} - L_{211}] \tilde{\Phi}_3^-(\mathbf{P}) \\ &+ V[L_{020} - L_{200}] \tilde{\Phi}_4^-(\mathbf{P}) \\ &+ V[L_{101} - L_{12\bar{1}}] \tilde{\Phi}_5^-(\mathbf{P}) \\ &+ V[L_{21\bar{1}} - L_{011}] \tilde{\Phi}_6^-(\mathbf{P}).\end{aligned}\quad (\text{A10})$$

$$\begin{pmatrix} V[L_{000} - L_{220}] & V[L_{10\bar{1}} - L_{121}] & V[L_{01\bar{1}} - L_{211}] & V[L_{020} - L_{200}] & V[L_{101} - L_{12\bar{1}}] & V[L_{21\bar{1}} - L_{011}] \\ V[L_{10\bar{1}} - L_{121}] & V[L_{000} - L_{022}] & V[L_{110} - L_{112}] & V[L_{1\bar{1}21} - L_{101}] & V[L_{002} - L_{020}] & V[L_{110} - L_{1\bar{1}12}] \\ V[L_{01\bar{1}} - L_{211}] & V[L_{110} - L_{112}] & V[L_{000} - L_{202}] & V[L_{011} - L_{21\bar{1}}] & V[L_{11\bar{1}2} - L_{110}] & V[L_{200} - L_{002}] \\ V[L_{020} - L_{200}] & V[L_{12\bar{1}} - L_{101}] & V[L_{01\bar{1}} - L_{21\bar{1}}] & V[L_{000} - L_{220}] & V[L_{121} - L_{10\bar{1}}] & V[L_{21\bar{1}} - L_{011}] \\ V[L_{10\bar{1}} - L_{121}] & V[L_{002} - L_{020}] & V[L_{112} - L_{110}] & V[L_{1\bar{1}21} - L_{10\bar{1}}] & V[L_{000} - L_{022}] & V[L_{112} - L_{1\bar{1}10}] \\ V[L_{21\bar{1}} - L_{011}] & V[L_{110} - L_{112}] & V[L_{200} - L_{002}] & V[L_{211} - L_{011}] & V[L_{1\bar{1}2} - L_{110}] & V[L_{000} - L_{202}] \end{pmatrix} \begin{pmatrix} \tilde{\Phi}_1^- \\ \tilde{\Phi}_2^- \\ \tilde{\Phi}_3^- \\ \tilde{\Phi}_4^- \\ \tilde{\Phi}_5^- \\ \tilde{\Phi}_6^- \end{pmatrix} = \begin{pmatrix} \tilde{\Phi}_1^- \\ \tilde{\Phi}_2^- \\ \tilde{\Phi}_3^- \\ \tilde{\Phi}_4^- \\ \tilde{\Phi}_5^- \\ \tilde{\Phi}_6^- \end{pmatrix}.\quad (\text{A11})$$

A.2. Pair energy for Γ point

At the Γ point,

$$\begin{aligned}L_{lmn}(0) &= \frac{1}{N} \sum_{\mathbf{q}'} \frac{e^{i\left(l\frac{q'_x}{2} + m\frac{q'_y}{2} + n\frac{q'_z}{2}\right)}}{E - 2\varepsilon_{\mathbf{q}'}} \\ &= - \int_{-2\pi}^{2\pi} \int_{-2\pi}^{2\pi} \int_{-2\pi}^{2\pi} \frac{dq'_x dq'_y dq'_z}{(4\pi)^3} \frac{\cos\left(l\frac{q'_x}{2}\right) \cos\left(m\frac{q'_y}{2}\right) \cos\left(n\frac{q'_z}{2}\right)}{|E| - 8t \left\{ \cos\left(\frac{q'_x}{2}\right) \cos\left(\frac{q'_y}{2}\right) + \cos\left(\frac{q'_x}{2}\right) \cos\left(\frac{q'_z}{2}\right) + \cos\left(\frac{q'_y}{2}\right) \cos\left(\frac{q'_z}{2}\right) \right\}} \\ &= - \frac{1}{(2\pi)^3} \int_{-\pi}^{\pi} \int_{-\pi}^{\pi} \int_{-\pi}^{\pi} \frac{\cos(lq''_x) \cos(mq''_y) \cos(nq''_z)}{|E| - 8t \left\{ \cos(q''_x) \cos(q''_y) + \cos(q''_x) \cos(q''_z) + \cos(q''_y) \cos(q''_z) \right\}} dq''_x dq''_y dq''_z : \left(q''_j = \frac{q'_j}{2} \right)\end{aligned}\quad (\text{A12})$$

Because some of the Green's functions are identical due to symmetry properties [41], we may then use the simplifications below

$$\begin{aligned}L_{000} &= L_0 \\ L_{110} &= L_{101} = L_{011} = L_{1\bar{1}01} = L_{01\bar{1}} = L_{10\bar{1}} \\ &= L_{10\bar{1}} = L_{01\bar{1}} = L_{01\bar{1}} = L_{110} = L_{1\bar{1}0} = L_{1\bar{1}0} \equiv L_1 \\ L_{220} &= L_{022} = L_{202} = L_{2\bar{2}0} = L_{02\bar{2}} = L_{20\bar{2}} \equiv L_2 \\ L_{200} &= L_{020} = L_{002} = L_{200} = L_{020} = L_{002} \equiv L_3 \\ L_{211} &= L_{121} = L_{112} = L_{211} = L_{121} = L_{112} = L_{1\bar{1}2} = L_{1\bar{1}2} = \dots \equiv L_4,\end{aligned}\quad (\text{A13})$$

to modify our dispersion matrices (A7) and (A11) to obtain (at the Γ point, $\tilde{\Phi}_i^\pm = \Phi_i^\pm$):

$$\underbrace{\begin{pmatrix} UL_0 & 2VL_1 & 2VL_1 & 2VL_1 & 2VL_1 & 2VL_1 & 2VL_1 \\ UL_1 & V[L_0 + L_2] & V[L_1 + L_4] & V[L_1 + L_4] & 2VL_3 & V[L_1 + L_4] & V[L_4 + L_1] \\ UL_1 & V[L_1 + L_4] & V[L_0 + L_2] & V[L_1 + L_4] & V[L_4 + L_1] & 2VL_3 & V[L_1 + L_4] \\ UL_1 & V[L_1 + L_4] & V[L_1 + L_4] & V[L_0 + L_2] & V[L_1 + L_4] & V[L_4 + L_1] & 2VL_3 \\ UL_1 & 2VL_3 & V[L_4 + L_1] & V[L_1 + L_4] & V[L_0 + L_2] & V[L_4 + L_1] & V[L_4 + L_1] \\ UL_1 & V[L_1 + L_4] & 2VL_3 & V[L_4 + L_1] & V[L_4 + L_1] & V[L_0 + L_2] & V[L_4 + L_1] \\ UL_1 & V[L_4 + L_1] & V[L_1 + L_4] & 2VL_3 & V[L_4 + L_1] & V[L_4 + L_1] & V[L_0 + L_2] \end{pmatrix}}_{\hat{L}_{\text{singlet}}} \underbrace{\begin{pmatrix} \Phi_0^+ \\ \Phi_1^+ \\ \Phi_2^+ \\ \Phi_3^+ \\ \Phi_4^+ \\ \Phi_5^+ \\ \Phi_6^+ \end{pmatrix}}_{\hat{\Phi}_{\text{singlet}}} = \underbrace{\begin{pmatrix} \Phi_0^+ \\ \Phi_1^+ \\ \Phi_2^+ \\ \Phi_3^+ \\ \Phi_4^+ \\ \Phi_5^+ \\ \Phi_6^+ \end{pmatrix}}_{\hat{\Phi}_{\text{singlet}}}, \quad (\text{A14})$$

$$\underbrace{\begin{pmatrix} V[L_0 - L_2] & V[L_1 - L_4] & V[L_1 - L_4] & 0 & V[L_1 - L_4] & V[L_4 - L_1] \\ V[L_1 - L_4] & V[L_0 - L_2] & V[L_1 - L_4] & V[L_4 - L_1] & 0 & V[L_1 - L_4] \\ V[L_1 - L_4] & V[L_1 - L_4] & V[L_0 - L_2] & V[L_1 - L_4] & V[L_4 - L_1] & 0 \\ 0 & V[L_4 - L_1] & V[L_1 - L_4] & V[L_0 - L_2] & V[L_4 - L_1] & V[L_4 - L_1] \\ V[L_1 - L_4] & 0 & V[L_4 - L_1] & V[L_4 - L_1] & V[L_0 - L_2] & V[L_4 - L_1] \\ V[L_4 - L_1] & V[L_1 - L_4] & 0 & V[L_4 - L_1] & V[L_4 - L_1] & V[L_0 - L_2] \end{pmatrix}}_{\hat{L}_{\text{triplet}}} \underbrace{\begin{pmatrix} \Phi_1^- \\ \Phi_2^- \\ \Phi_3^- \\ \Phi_4^- \\ \Phi_5^- \\ \Phi_6^- \end{pmatrix}}_{\hat{\Phi}_{\text{triplet}}} = \underbrace{\begin{pmatrix} \Phi_1^- \\ \Phi_2^- \\ \Phi_3^- \\ \Phi_4^- \\ \Phi_5^- \\ \Phi_6^- \end{pmatrix}}_{\hat{\Phi}_{\text{triplet}}}. \quad (\text{A15})$$

We may rewrite the matrices above as

$$\hat{L}_{s,t} \hat{\Phi}_{s,t} = \lambda_{s,t} \hat{\Phi}_{s,t}, \quad (\text{A16})$$

to form an eigenvalue problem where \hat{L}_s and \hat{L}_t are the singlet and triplet dispersion matrices, λ_s and λ_t being the eigenvalues corresponding to singlet $\hat{\Phi}_s$ and triplet $\hat{\Phi}_t$ eigenvectors, respectively. To find the pair energy, we select E , compute L and then λ . A true pair state corresponds to $\lambda = 1$. Thus, all pair energies can be found by adjusting E and searching for $\lambda = 1$ using standard binary search algorithms.

As the Green's functions and dispersion matrices become more simplified at the Γ point of the FCC lattice, one can take further advantage of this high symmetry point. We use this point to evaluate the binding conditions for the formation of the bound states (with s -, p -, $d_{T_{2g}}$ -, d_{E_g} - and f - symmetries). Via the irreducible representations of the O_h group [42], we can determine some linear combinations (excluding the normalisation constants) of the eigenvector by performing the 48 operations on the FCC lattice. Note that the eigenfunction Φ_0^+ is at the centre of zone and therefore remains unchanged due to the operations. These operations yield the irreducible representations for both the singlet and triplet states as

$$\begin{aligned} \Gamma_{\text{singlet}}^{\text{fcc}} &= A_{1g} \oplus E_g \oplus T_{2g} \\ \Gamma_{\text{triplet}}^{\text{fcc}} &= T_{1u} \oplus T_{2u} \end{aligned} \quad (\text{A17})$$

A_{1g} is s -symmetrical, E_g and T_{2g} are of d -symmetry, T_{1u} has p -symmetry while T_{2u} forms an f -symmetric state. An example of a symmetrised linear combinations for the singlets is

$$\chi^{A_{1g}} = \Phi_1^+ + \Phi_2^+ + \Phi_3^+ + \Phi_4^+ + \Phi_5^+ + \Phi_6^+, \quad (\text{A18})$$

$$\chi^{T_{2g}} = \begin{cases} \Phi_1^+ - \Phi_4^+ \\ \Phi_3^+ - \Phi_6^+ \\ \Phi_2^+ - \Phi_5^+ \end{cases}, \quad (\text{A19})$$

$$\chi^{E_g} = \begin{cases} \Phi_1^+ - 2\Phi_2^+ + \Phi_3^+ + \Phi_4^+ - 2\Phi_5^+ + \Phi_6^+ \\ \Phi_1^+ - \Phi_3^+ + \Phi_4^+ - \Phi_6^+ \end{cases}, \quad (\text{A20})$$

and for the triplets is

$$\chi^{T_{1u}} = \begin{cases} \Phi_1^- + \Phi_2^- - \Phi_4^- + \Phi_5^- \\ \Phi_1^- + \Phi_3^- + \Phi_4^- - \Phi_6^- \\ -\Phi_2^- - \Phi_3^- + \Phi_5^- - \Phi_6^- \end{cases}, \quad (\text{A21})$$

$$\chi^{T_{2u}} = \begin{cases} \Phi_2^- - \Phi_3^- - \Phi_5^- - \Phi_6^- \\ \Phi_1^- - \Phi_3^- + \Phi_4^- + \Phi_6^- \\ \Phi_1^- - \Phi_2^- - \Phi_4^- - \Phi_5^- \end{cases}. \quad (\text{A22})$$

Allowing transformation to a new orthogonal basis [43, 44]

$$\begin{pmatrix} \Phi_0 \\ \Phi_s \\ \Phi_{d_1} \\ \Phi_{d_2} \\ \Phi_{d_3} \\ \Phi_{d_4} \\ \Phi_{d_5} \end{pmatrix} = \begin{pmatrix} 1 & 0 & 0 & 0 & 0 & 0 & 0 \\ 0 & 1 & 1 & 1 & 1 & 1 & 1 \\ 0 & 1 & 0 & 0 & -1 & 0 & 0 \\ 0 & 0 & 0 & 1 & 0 & 0 & -1 \\ 0 & 0 & 1 & 0 & 0 & -1 & 0 \\ 0 & 1 & -2 & 1 & 1 & -2 & 1 \\ 0 & 1 & 0 & -1 & 1 & 0 & -1 \end{pmatrix} \begin{pmatrix} \Phi_0^+ \\ \Phi_1^+ \\ \Phi_2^+ \\ \Phi_3^+ \\ \Phi_4^+ \\ \Phi_5^+ \\ \Phi_6^+ \end{pmatrix} \equiv \hat{\chi}_s \begin{pmatrix} \Phi_0^+ \\ \Phi_1^+ \\ \Phi_2^+ \\ \Phi_3^+ \\ \Phi_4^+ \\ \Phi_5^+ \\ \Phi_6^+ \end{pmatrix}, \quad (\text{A23})$$

$$\begin{pmatrix} \Phi_{p_1} \\ \Phi_{p_2} \\ \Phi_{p_3} \\ \Phi_{f_1} \\ \Phi_{f_2} \\ \Phi_{f_3} \end{pmatrix} = \begin{pmatrix} 1 & 1 & 0 & -1 & 1 & 0 \\ 1 & 0 & 1 & 1 & 0 & -1 \\ 0 & -1 & -1 & 0 & 1 & -1 \\ 0 & 1 & -1 & 0 & -1 & -1 \\ 1 & 0 & -1 & 1 & 0 & 1 \\ 1 & -1 & 0 & -1 & -1 & 0 \end{pmatrix} \begin{pmatrix} \Phi_1^- \\ \Phi_2^- \\ \Phi_3^- \\ \Phi_4^- \\ \Phi_5^- \\ \Phi_6^- \end{pmatrix} \equiv \hat{\chi}_t \begin{pmatrix} \Phi_1^- \\ \Phi_2^- \\ \Phi_3^- \\ \Phi_4^- \\ \Phi_5^- \\ \Phi_6^- \end{pmatrix}. \quad (\text{A24})$$

We diagonalise the equation using

$$\hat{L}_i^{\text{diag}} = \hat{\chi}_i \cdot \hat{L}_i \cdot \hat{\chi}_i^{-1}. \quad (\text{A25})$$

The respective block-diagonal self-consistent equations are

$$\begin{pmatrix} UL_0 & 2VL_1 & 0 & 0 & 0 & 0 & 0 \\ 6UL_1 & \mathcal{K}_s & 0 & 0 & 0 & 0 & 0 \\ 0 & 0 & \mathcal{K}_{dT_{2g}} & 0 & 0 & 0 & 0 \\ 0 & 0 & 0 & \mathcal{K}_{dT_{2g}} & 0 & 0 & 0 \\ 0 & 0 & 0 & 0 & \mathcal{K}_{dT_{2g}} & 0 & 0 \\ 0 & 0 & 0 & 0 & 0 & \mathcal{K}_{dE_g} & 0 \\ 0 & 0 & 0 & 0 & 0 & 0 & \mathcal{K}_{dE_g} \end{pmatrix} \begin{pmatrix} \Phi_0 \\ \Phi_s \\ \Phi_{d_1} \\ \Phi_{d_2} \\ \Phi_{d_3} \\ \Phi_{d_4} \\ \Phi_{d_5} \end{pmatrix} = \begin{pmatrix} \Phi_0 \\ \Phi_s \\ \Phi_{d_1} \\ \Phi_{d_2} \\ \Phi_{d_3} \\ \Phi_{d_4} \\ \Phi_{d_5} \end{pmatrix}, \quad (\text{A26})$$

$$\begin{pmatrix} \mathcal{K}_p & 0 & 0 & 0 & 0 & 0 \\ 0 & \mathcal{K}_p & 0 & 0 & 0 & 0 \\ 0 & 0 & \mathcal{K}_p & 0 & 0 & 0 \\ 0 & 0 & 0 & \mathcal{K}_f & 0 & 0 \\ 0 & 0 & 0 & 0 & \mathcal{K}_f & 0 \\ 0 & 0 & 0 & 0 & 0 & \mathcal{K}_f \end{pmatrix} \begin{pmatrix} \Phi_{p_1} \\ \Phi_{p_2} \\ \Phi_{p_3} \\ \Phi_{f_1} \\ \Phi_{f_2} \\ \Phi_{f_3} \end{pmatrix} = \begin{pmatrix} \Phi_{p_1} \\ \Phi_{p_2} \\ \Phi_{p_3} \\ \Phi_{f_1} \\ \Phi_{f_2} \\ \Phi_{f_3} \end{pmatrix}, \quad (\text{A27})$$

where

$$\begin{aligned} \mathcal{K}_s &= V[L_0 + 4L_1 + L_2 + 2L_3 + 4L_4] \\ \mathcal{K}_{dT_{2g}} &= V[L_0 + L_2 - 2L_3] \\ \mathcal{K}_{dE_g} &= V[L_0 - 2L_1 + L_2 + 2L_3 - 2L_4] \\ \mathcal{K}_p &= V[L_0 + 2L_1 - L_2 - 2L_4] \\ \mathcal{K}_f &= V[L_0 - 2L_1 - L_2 + 2L_4]. \end{aligned}$$

These are the solutions to the two-body problem at $\mathbf{P} = 0$. The 2×2 block in equation (A26) corresponds to the s -symmetrical state, the next three 1×1 blocks are triply degenerate d -states of T_{2g} symmetry and the last two are another doubly degenerate d -states with the E_g symmetry. In the case of spin triplet states in equation (A27), the p - and f - states are three-fold degenerate and they belong to the T_{1u} and T_{2u} symmetry respectively.

It is possible to evaluate the exact binding threshold for the emergence of a bound state. With the symmetrised and diagonalised equations, we set the energy value as $E \rightarrow -2W = -24t$. The self-consistent equations give

$$s: \quad \begin{pmatrix} 1 - UL_0 & -2VL_1 \\ -6UL_1 & 1 - \mathcal{K}_s \end{pmatrix} = 0. \quad (\text{A28})$$

$$dT_{2g}: \quad 1 - \mathcal{K}_{dT_{2g}} = 0, \quad (\text{A29})$$

$$dE_g: \quad 1 - \mathcal{K}_{dE_g} = 0, \quad (\text{A30})$$

$$p: \quad 1 - \mathcal{K}_p = 0, \quad (\text{A31})$$

$$f: \quad 1 - \mathcal{K}_f = 0. \quad (\text{A32})$$

Following reference [45], the exact solution of the Green's functions in equation (A13) are

$$L_0 = -\frac{\sqrt{3}K_0^2}{8\pi^2 t} = \frac{-0.056\,027\,549\,298\,548}{t}, \quad (\text{A33})$$

$$L_1 = \frac{1}{24t} - \frac{\sqrt{3}K_0^2}{8\pi^2 t} = \frac{1}{24t} + L_0, \quad (\text{A34})$$

$$L_2 = -\frac{9\sqrt{3}K_0^2}{8\pi^2 t} - \frac{3}{4t\sqrt{3}K_0^2} + \frac{2}{3t} = 9L_0 + \frac{3}{32\pi^2 t^2 L_0} + \frac{2}{3t}, \quad (\text{A35})$$

$$L_3 = \frac{\sqrt{3}K_0^2}{24\pi^2 t} - \frac{1}{8t\sqrt{3}K_0^2} = \frac{1}{64\pi^2 t^2 L_0} - \frac{L_0}{3}, \quad (\text{A36})$$

$$L_4 = \frac{\sqrt{3}K_0^2}{24\pi^2 t} + \frac{1}{4t\sqrt{3}K_0^2} - \frac{1}{12t} = -\frac{L_0}{3} - \frac{1}{32\pi^2 t^2 L_0} - \frac{1}{12t}, \quad (\text{A37})$$

where the complete elliptic integral of the first kind $K_0 = K\left(\frac{\sqrt{3}-1}{2\sqrt{2}}\right) = 1.598\,142\,002\,112\,540$.

The binding conditions are obtained from equations (A28)–(A32) to be

$$V_c^s \leq V(U) = \frac{UL_0 - 1}{UL_0 C - C - 12UL_1^2}, \quad (\text{A38})$$

where $C = L_0 + 4L_1 + L_2 + 2L_3 + 4L_4 = 12L_0 + \frac{1}{2t} = -0.172\,330\,591\,582\,576/t$.

$$V_c^{d_{T2g}} = -22.734\,195\,989\,010\,747t, \quad (\text{A39})$$

$$V_c^{d_{Eg}} = -26.810\,644\,276\,320\,041t, \quad (\text{A40})$$

$$V_c^p = -16.302\,567\,033\,831\,927t, \quad (\text{A41})$$

$$V_c^f = -27.416\,574\,191\,996\,979t. \quad (\text{A42})$$

In specific limits, the critical binding of s -states is

$$V_c^s(U=0) = -5.80\,280\,025t, \quad (\text{A43})$$

$$V_c^s(U \rightarrow +\infty) = -7.8\,028\,002\,504t, \quad (\text{A44})$$

$$U_c(V=0) = -17.84\,836\,232\,388t, \quad (\text{A45})$$

$$U_c(V \rightarrow +\infty) = -24t. \quad (\text{A46})$$

Appendix B. Pair mass in the superlight limit

Expanding the one-particle dispersion at small \mathbf{k} , one obtains

$$\varepsilon_{\mathbf{k}} \approx -12t + tb^2(k_x^2 + k_y^2 + k_z^2) = \varepsilon_0 + \frac{\hbar^2}{2m_0}(k_x^2 + k_y^2 + k_z^2), \quad (\text{B1})$$

where $m_0 = \hbar^2/(2tb^2)$ is the free particle mass.

We define six singlet dimer basis states

$$D_{i,\mathbf{n}} = \frac{1}{\sqrt{2}} \left(|\uparrow\rangle_{\mathbf{n}} |\downarrow\rangle_{\mathbf{n}+\mathbf{a}_i} + |\downarrow\rangle_{\mathbf{n}} |\uparrow\rangle_{\mathbf{n}+\mathbf{a}_i} \right). \quad (\text{B2})$$

$D_{i,\mathbf{n}}$ are the only states with nonzero weights in the $V \rightarrow -\infty$ limit. Because of the topology of the FCC lattice, $D_{i,\mathbf{n}}$ are linked by first-order hopping events. The first-order Hamiltonian matrix is

$$\hat{H}D_{1,\mathbf{n}} = -t(D_{3,\mathbf{n}} + D_{3,\mathbf{n}+\mathbf{a}_6}) - t(D_{4,\mathbf{n}} + D_{4,\mathbf{n}+\mathbf{a}_5}) - t(D_{5,\mathbf{n}} + D_{5,\mathbf{n}+\mathbf{a}_4}) - t(D_{6,\mathbf{n}} + D_{6,\mathbf{n}+\mathbf{a}_3}), \quad (\text{B3})$$

$$\hat{H}D_{2,\mathbf{n}} = -t(D_{3,\mathbf{n}} + D_{3,\mathbf{n}-\mathbf{a}_5}) - t(D_{4,\mathbf{n}} + D_{4,\mathbf{n}-\mathbf{a}_6}) - t(D_{5,\mathbf{n}+\mathbf{a}_2} + D_{5,\mathbf{n}-\mathbf{a}_5}) - t(D_{6,\mathbf{n}+\mathbf{a}_2} + D_{6,\mathbf{n}-\mathbf{a}_6}), \quad (\text{B4})$$

$$\hat{H}D_{3,\mathbf{n}} = -t(D_{1,\mathbf{n}} + D_{1,\mathbf{n}-\mathbf{a}_6}) - t(D_{2,\mathbf{n}} + D_{2,\mathbf{n}+\mathbf{a}_5}) - t(D_{5,\mathbf{n}} + D_{5,\mathbf{n}+\mathbf{a}_2}) - t(D_{6,\mathbf{n}+\mathbf{a}_3} + D_{6,\mathbf{n}-\mathbf{a}_6}), \quad (\text{B5})$$

$$\hat{H}D_{4,\mathbf{n}} = -t(D_{1,\mathbf{n}} + D_{1,\mathbf{n}+\mathbf{a}_2}) - t(D_{2,\mathbf{n}} + D_{2,\mathbf{n}+\mathbf{a}_6}) - t(D_{5,\mathbf{n}-\mathbf{a}_5} + D_{5,\mathbf{n}+\mathbf{a}_4}) - t(D_{6,\mathbf{n}} + D_{6,\mathbf{n}+\mathbf{a}_2}), \quad (\text{B6})$$

$$\hat{H}D_{5,\mathbf{n}} = -t(D_{1,\mathbf{n}} + D_{1,\mathbf{n}-\mathbf{a}_4}) - t(D_{2,\mathbf{n}-\mathbf{a}_2} + D_{2,\mathbf{n}+\mathbf{a}_5}) - t(D_{3,\mathbf{n}} + D_{3,\mathbf{n}-\mathbf{a}_2}) - t(D_{4,\mathbf{n}-\mathbf{a}_4} + D_{4,\mathbf{n}+\mathbf{a}_5}), \quad (\text{B7})$$

$$\hat{H}D_{6,\mathbf{n}} = -t(D_{1,\mathbf{n}} + D_{1,\mathbf{n}-\mathbf{a}_3}) - t(D_{2,\mathbf{n}-\mathbf{a}_2} + D_{2,\mathbf{n}+\mathbf{a}_6}) - t(D_{3,\mathbf{n}+\mathbf{a}_6} + D_{3,\mathbf{n}-\mathbf{a}_3}) - t(D_{4,\mathbf{n}} + D_{4,\mathbf{n}-\mathbf{a}_2}). \quad (\text{B8})$$

Applying a Fourier transform one obtains the dimer Schrödinger equation. Its self-consistent condition yields pair energy E for a given pair momentum \mathbf{P} .

$$\begin{vmatrix}
 E & 0 & t(1 + e^{iPa_6}) & t(1 + e^{iPa_5}) & t(1 + e^{iPa_4}) & t(1 + e^{iPa_3}) \\
 0 & E & t(1 + e^{-iPa_6}) & t(1 + e^{-iPa_5}) & t(e^{iPa_2} + e^{-iPa_5}) & t(e^{iPa_2} + e^{-iPa_6}) \\
 t(1 + e^{-iPa_6}) & t(1 + e^{iPa_5}) & E & 0 & t(1 + e^{iPa_2}) & t(e^{iPa_3} + e^{-iPa_6}) \\
 t(1 + e^{-iPa_5}) & t(1 + e^{iPa_6}) & 0 & E & t(e^{iPa_4} + e^{-iPa_5}) & t(1 + e^{iPa_2}) \\
 t(1 + e^{-iPa_4}) & t(e^{iPa_5} + e^{-iPa_2}) & t(1 + e^{-iPa_2}) & t(e^{iPa_5} + e^{-iPa_4}) & E & 0 \\
 t(1 + e^{-iPa_3}) & t(e^{iPa_6} + e^{-iPa_2}) & t(e^{iPa_6} + e^{-iPa_3}) & t(1 + e^{-iPa_2}) & 0 & E
 \end{vmatrix} = 0. \quad (B9)$$

The general dispersion equation (B9) is too complex. However, to extract a pair mass it is sufficient to know $E(\mathbf{P})$ at small \mathbf{P} . Utilising the isotropy property of cubic dispersion relations, we set $\mathbf{P} = (P_x, 0, 0)$ and expand equation (B9) to get

$$E^3(E - 4t) \left[E^2 + 4tE - 16t^2 \left(1 + \cos \frac{P_x b}{2} \right) \right] = 0, \quad (B10)$$

which defines dispersion of six pair bands along the P_x direction. The lowest band is

$$E_1(P_x) = -2t \left(1 + \sqrt{5 + 4 \cos \frac{P_x b}{2}} \right). \quad (B11)$$

Expanding at small P_x , one obtains

$$E_1(P_x b \ll 1) \approx -8t + \frac{1}{6} t(P_x b)^2 \equiv E_0 + \frac{\hbar^2 P_x^2}{2 m^*}, \quad (B12)$$

from where

$$m^* = \frac{3\hbar^2}{tb^2} = 6m_0. \quad (B13)$$

Thus even an infinitely bound intersite pair is only six times heavier than a free particle.

ORCID iDs

G D Adebajo  <https://orcid.org/0000-0002-5835-8860>
 P E Kornilovitch  <https://orcid.org/0000-0002-4632-8779>
 J P Hague  <https://orcid.org/0000-0002-5760-8696>

References

- [1] Hague J P, Kornilovitch P E, Samson J H and Alexandrov A S 2007 Superlight small bipolarons *J. Phys.: Condens. Matter.* **19** 255214
- [2] Hague J P, Kornilovitch P E, Samson J H and Alexandrov A S 2007 Superlight small bipolarons in the presence of a strong Coulomb repulsion *Phys. Rev. Lett.* **98** 037002
- [3] Hague J P, Kornilovitch P E, Samson J H and Alexandrov A S 2008 Singlet and triplet bipolarons on the triangular lattice *J. Phys. Chem. Solids* **69** 3304–6
- [4] Hague J P and Kornilovitch P E 2010 Light and stable triplet bipolarons on square and triangular lattices *Phys. Rev. B* **82** 094301
- [5] Hirsch J E 1984 Charge-density-wave to spin-density-wave transition in the extended Hubbard model *Phys. Rev. Lett.* **53** 2327–30
- [6] Micnas R, Ranninger J and Robaszkiewicz S 1990 Superconductivity in narrow-band systems with local nonretarded attractive interactions *Rev. Mod. Phys.* **62** 113–71
- [7] Kornilovitch P 2004 Enhanced stability of bound pairs at nonzero lattice momenta *Phys. Rev. B* **69** 235110
- [8] Bak M 2007 Bound electron pairs on a triangular lattice in an extended Hubbard model *Phys. Status Solidi b* **244** 2421–6
- [9] Davenport A R, Hague J P and Kornilovitch P E 2012 Mobile small bipolarons on a three-dimensional cubic lattice *Phys. Rev. B* **86** 035106
- [10] Adebajo G D, Kornilovitch P E and Hague J P 2021 Fermion pairing in body-centered-cubic quantum simulators of extended Hubbard models *Phys. Lett. A* **418** 127704
- [11] Ranninger J and Robaszkiewicz S 1988 An extended Hubbard model with inter-site attraction in two dimensions and high- T_c superconductivity *J. Phys. C: Solid State Phys.* **21** L145–51
- [12] Jiang M, Hähner U R, Schulthess T C and Maier T A 2018 d -wave superconductivity in the presence of nearest-neighbor Coulomb repulsion *Phys. Rev. B* **97** 184507
- [13] Hardy T M, Hague J P, Samson J H and Alexandrov A S 2009 Superconductivity in a Hubbard–Fröhlich model and in cuprates *Phys. Rev. B* **79** 212501
- [14] Spałek J, Zegrodnik M and Kaczmarczyk J 2017 Universal properties of high-temperature superconductors from real-space pairing: t - J - U model and its quantitative comparison with experiment *Phys. Rev. B* **95** 024506
- [15] Qu D-W, Chen B-B, Jiang H-C, Wang Y and Li W 2021 Spin-triplet pairing induced by near-neighbor attraction in the cuprate chain (arXiv:2110.00564)
- [16] Hubbard J 1963 Electron correlations in narrow energy bands *Proc. R. Soc. A* **276** 238–57
- [17] Laad M S and Ghosh D K 1991 Extended Hubbard model in two dimensions *J. Phys.: Condens. Matter.* **3** 9723–32
- [18] Kato T and Kato M 2000 Stripe orders in the extended Hubbard model *J. Phys. Soc. Japan* **69** 3972–9
- [19] Chen Z *et al* 2021 Anomalously strong near-neighbor attraction in doped 1D cuprate chains *Science* **373** 1235–9
- [20] Wang Y, Chen Z, Shi T, Moritz B, Shen Z-X and Devereaux T P 2021 Phonon-mediated long-range attractive interaction in one-dimensional cuprates *Phys. Rev. Lett.* **127** 197003
- [21] Arrachea L and Aligia A A 2004 d -wave superconductivity in the effective extended Hubbard model for cuprates *Physica C* **408–410** 224–5
- [22] Schollwöck U 2011 The density-matrix renormalization group in the age of matrix product states *Ann. Phys., NY* **326** 96–192
- [23] Glocke S, Klümper A and Sirker J 2007 Half-filled one-dimensional extended Hubbard model: phase diagram and thermodynamics *Phys. Rev. B* **76** 155121

- [24] Georges A, Kotliar G, Krauth W and Rozenberg M J 1996 Dynamical mean-field theory of strongly correlated fermion systems and the limit of infinite dimensions *Rev. Mod. Phys.* **68** 13–125
- [25] Maier T, Jarrell M, Pruschke T and Hettler M H 2005 Quantum cluster theories *Rev. Mod. Phys.* **77** 1027–80
- [26] Medvedeva D, Isakov S, Krien F, Mazurenko V V and Lichtenstein A I 2017 Exact diagonalization solver for extended dynamical mean-field theory *Phys. Rev. B* **96** 235149
- [27] Sheridan E, Weber C, Plekhanov E and Rhodes C 2019 Continuous-time quantum Monte Carlo solver for dynamical mean field theory in the compact Legendre representation *Phys. Rev. B* **99** 205156
- [28] Lupo C, Jamet F, Tse W H T, Rungger I and Weber C 2021 Maximally localized dynamical quantum embedding for solving many-body correlated systems *Nat. Comput. Sci.* **1** 410–20
- [29] Lee H, Plekhanov E, Blackburn D, Acharya S and Weber C 2019 The Mott to Kondo transition in diluted Kondo superlattices *Commun. Physics* **2** 49
- [30] al-Badri M A, Linscott E, Georges A, Cole D J and Weber C 2020 Superexchange mechanism and quantum many body excitations in the archetypal di-Cu oxo-bridge *Commun. Phys.* **3** 4
- [31] Sheridan E, Rhodes C, Jamet F, Rungger I and Weber C 2021 Data-driven dynamical mean-field theory: an error-correction approach to solve the quantum many-body problem using machine learning *Phys. Rev. B* **104** 205120
- [32] Linscott E B, Cole D J, Hine N D M, Payne M C and Weber C 2020 ONETEP + TOSCAM: uniting dynamical mean field theory and linear-scaling density functional theory *J. Chem. Theory Comput.* **16** 4899–911
- [33] Gunnarsson O 1997 Superconductivity in fullerenes *Rev. Mod. Phys.* **69** 575–606
- [34] Gunnarsson O 2004 *Alkali-Doped Fullerenes: Narrow-Band Solids with Unusual Properties* (Singapore: World Scientific)
- [35] Capone M, Fabrizio M, Castellani C and Tosatti E 2009 Colloquium: modeling the unconventional superconducting properties of expanded A_3C_{60} fullerenes *Rev. Mod. Phys.* **81** 943–58
- [36] Takada Y and Hotta T 1998 Superconductivity in the alkali-doped fullerenes: competition of phonon-mediated attractions with Coulomb repulsions in polaron pairing *Int. J. Mod. Phys. B* **12** 3042–51
- [37] Byczuk K, Spałek J and Wójcik W 1992 Microscopic model of hybrid pairing: II. Exact solution for a single pair *Phys. Rev. B* **46** 14134–41
- [38] Padilla W J, Lee Y S, Dumm M, Blumberg G, Ono S, Segawa K, Komiyama S, Ando Y and Basov D N 2005 Constant effective mass across the phase diagram of high- T_c cuprates *Phys. Rev. B* **72** 060511
- [39] Lang L J, Zhang S L, Law K T and Zhou Q 2017 Weyl points and topological nodal superfluids in a face-centered-cubic optical lattice *Phys. Rev. B* **96** 035145
- [40] Yuan L, Wang G P and Huang X 2003 Arrangements of four beams for any Bravais lattice *Opt. Lett.* **28** 1769–71
- [41] Morita T 1975 Use of a recurrence formula in computing the lattice Green function *J. Phys. A: Math. Gen.* **8** 478–89
- [42] Cornwell J F 1997 Appendix C—character tables for the crystallographic point groups *Group Theory in Physics: An Introduction (Techniques of Physics vol 1)* (New York: Academic) pp 299–318
- [43] The normalisation factors have been omitted.
- [44] The subscript s is used twice: Φ_s means all possible singlet states (s, d, d^*) while Φ_s means an s -state only.
- [45] Glasser M L and Boersma J 2000 Exact values for the cubic lattice Green functions *J. Phys. A: Math. Gen.* **33** 5017